TURUN
YLIOPISTO
UNIVERSITY
OF TURKU

WHERE ARE THE STARS OF YESTERYEAR?

A Reflection on Astrophysical Transience

Shane Moran

TURUN YLIOPISTON JULKAISUJA – ANNALES UNIVERSITATIS TURKUENSIS
SARJA – SER. AI OSA – TOM. 731 | ASTRONOMICA – CHEMICA – PHYSICA – MATHEMATICA | TURKU 2025

TURUN
YLIOPISTO
UNIVERSITY
OF TURKU

WHERE ARE THE STARS OF YESTERYEAR?

A Reflection on Astrophysical Transience

Shane Moran

TURUN YLIOPISTON JULKAISUJA – ANNALES UNIVERSITATIS TURKUENSIS
SARJA – SER. AI OSA – TOM. 731 | ASTRONOMICA – CHEMICA – PHYSICA – MATHEMATICA | TURKU 2025

University of Turku

Faculty of Science
Department of Physics and Astronomy
Astronomy
Doctoral Programme in Exact Sciences (EXACTUS)

Supervised by

Doc. Rubina Kotak
Department of Physics and Astronomy
University of Turku
Turku, Finland

Assist. Prof. Morgan Fraser
School of Physics
University College Dublin
Dublin, Ireland

Prof. Seppo Mattila
Department of Physics and Astronomy
University of Turku
Turku, Finland

Reviewed by

Dr. Stacey Habergham-Mawson
Astrophysics Research Institute
Liverpool John Moores University
Liverpool, United Kingdom

Dr. Heidi Korhonen
Technical Departments
Max Planck Institute for Astronomy
Heidelberg, Germany

Opponent

Dr. Jonathan Mackey
Dunsink Observatory
Dublin Institute for Advanced Studies
Dublin, Ireland

ISBN 978-952-02-0052-7 (PRINT)
ISBN 978-952-02-0053-4 (PDF)
ISSN 0082-7002 (PRINT)
ISSN 2343-3175 (ONLINE)
Painosalama, Turku, Finland, 2025

In memory of David Tims

UNIVERSITY OF TURKU
Faculty of Science
Department of Physics and Astronomy
Astronomy
MORAN, SHANE: Where Are the Stars of Yesteryear?
Doctoral dissertation, 104 pp.
Doctoral Programme in Exact Sciences (EXACTUS)
January 2025

ABSTRACT

This thesis concerns a number of kinds of astrophysical transients, including interacting supernovae (SNe), gap transients and tidal-disruption events. There are three papers included and they address differing phenomena, each of which has implications for stellar evolution more broadly.

The first paper is a detailed study of the long-lived slowly evolving type IIn SN, SN 2017hcc. The paper covers a five-year follow-up campaign, with extensive optical and near-infrared imaging and spectroscopy. The object was very bright, peaking at -20.78 ± 0.01 mag in ATLAS o band after an eight-week rise, suggesting significant interaction between the ejecta and circumstellar material. The paper also covers evidence for pre-existing dust as well as new dust formation. The second paper is a study of the intermediate-luminosity red transient (ILRT), AT 2022fnm. This ILRT displayed certain features consistent with luminous red novae (LRNe) and the overlapping observational features of ILRTs and LRNe are discussed. The third paper concerns the fast-evolving transient SN 2017fwm/Gaia17byh. This object had an extremely fast rise time ($\lesssim$5 days) as well as a small ejecta mass ($0.01\,\mathrm{M}_{\odot}$). One particularly interesting feature of this object is that it displayed a peculiar velocity of approximately $-5000\,\mathrm{km\ s^{-1}}$. A number of origin scenarios for SN 2017fwm are explored in the paper, including its being an ultrastripped SN and its resulting from the tidal disruption of a white dwarf.

Additionally, upcoming astronomical surveys are discussed as well as the future of astronomical modelling and multi-messenger astronomy.

TURUN YLIOPISTO
Matemaattis-luonnontieteellinen tiedekunta
Fysiikan ja tähtitieteen laitos
Tähtitiede
MORAN, SHANE: Where Are the Stars of Yesteryear?
Väitöskirja, 104 s.
Eksaktien tieteiden tohtoriohjelma (EXACTUS)
Tammikuu 2025

TIIVISTELMÄ

Tämä väitöskirja käsittelee useita eri tyyppisiä astrofysikaalisia transientteja, mukaan lukien vuorovaikuttavat supernovat (SN), gap-transientit ja tähtien hajoamiset mustan aukon vuorovesivoimien vaikutuksesta (TDE, tidal-disruption event). Väitöskirjaan sisältyy kolme artikkelia, jotka käsittelevät erilaisia ilmiöitä, joilla on vaikutuksia tähtien kehitykseen laajemmin.

Ensimmäinen artikkeli on yksityiskohtainen tutkimus pitkäikäisestä, hitaasti kehittyvästä tyypin IIn SN:sta, SN 2017hcc. Artikkeli kattaa viiden vuoden seurantakampanjan, johon sisältyy laajaa optisen ja lähi-infrapuna-alueen kuvantamista ja spektroskopiaa. Kohde oli erittäin kirkas, saavuttaen huippu kirkkauden -20.78 ± 0.01 mag ATLASin o-kaistalla kahdeksan viikon nousun jälkeen, mikä viittaa merkittävään vuorovaikutukseen ulosvirtaavan ja ympäröivän aineen välillä. Artikkeli käsittelee myös todisteita jo olemassa olleesta pölystä sekä uuden pölyn muodostumisesta. Toinen artikkeli on tutkimus keskikirkkaasta punaisesta transientista (ILRT, intermediate-luminosity red transient), AT 2022fnm. Tämä ILRT osoitti tiettyjä ominaisuuksia, jotka olivat yhteensopivia kirkkaiden punaisten novien (LRN, luminous red nova) kanssa, ja artikkelissa käsitellään ILRT ja LRNe havaintojen yhteneväisyyksiä. Kolmas artikkeli käsittelee nopeasti kehittyvää transienttia SN 2017fwm/Gaia17byh. Tällä kohteella oli poikkeuksellisen nopea nousuaika ($\lesssim$5 päivää) sekä pieni ulosvirtausmassa ($0.01\,\mathrm{M}_\odot$). Yksi erityisen mielenkiintoinen piirre tässä kohteessa oli sen poikkeuksellinen nopeus $\sim -5000\,\mathrm{km\ s^{-1}}$. Artikkelissa tutkitaan useita SN 2017fwm:n syntyskenaarioita, kuten ultrastripped SN, tai valkoisen kääpiön aiheuttama TDE.

Lisäksi työssä pohditaan tulevia tähtitieteellisiä havainto-ohjelmia sekä tähtitieteellisen mallinnuksen ja moni-ilmaisinhavaintojen tulevaisuutta.

Acknowledgments

My sincere thanks to my supervisors, Rubina Kotak, Morgan Fraser and Seppo Mattila, for their invaluable guidance on research and academic matters throughout the PhD process. I would also like to thank the staff and students at the Nordic Optical Telescope in La Palma for an unforgettable time.

I wish to thank my pre-examiners, Stacey Habergham-Mawson and Heidi Korhonen, for their careful reading of the manuscript, as well my opponent, Jonathan Mackey, for his willingness to take part in my defence. The supernova group in the School of Physics at University College Dublin and the supernova group at the University of Turku also have my gratitude for very productive discussions and assistance. I also thank Christian Vassallo for translating the abstract of this thesis. I acknowledge the Magnus Ehrnrooth Foundation and the Vilho, Yrjö and Kalle Väisälä Foundation for providing financial support for the research contained in this thesis.

Finally, I must thank my friends and family, in particular, my mother, Teresa, whose unwavering encouragement I have cherished.

17th December 2024
Shane Moran

Table of Contents

Abbreviations

4MOST	4-metre Multi-Object Spectrograph Telescope
AGB	Asymptotic giant branch
BH	Black hole
CCSN	Core-collapse SN
CDS	Cool/cold dense shell
CSM	Circumstellar material
ECSN	Electron-capture supernova
ILRT	Intermediate-luminosity red transient
IMBH	Intermediate-mass black hole
LRN	Luminous red nova
LSST	Legacy Survey of Space and Time
NOT	Nordic Optical Telescope
NS	Neutron star
sAGB	Super-asymptotic giant branch star
SMBH	Supermassive black hole
SN	Supernova
SoXS	Son of X-Shooter
TDE	Tidal-disruption event
TiDES	Time-Domain Extragalactic Survey
USSN	Ultrastripped supernova
WD	White dwarf
ZAMS	Zero-age main sequence

List of Original Publications

This dissertation is based on the following original publications, which are referred to in the text by their Roman numerals:

I Moran, S., Fraser, M., Kotak, R., Pastorello, A., Benetti, S., Brennan, S. J., Gutiérrez, C. P., Kankare, E., Kuncarayakti, H., Mattila, S., Reynolds, T. M., Anderson, J. P., Brown, P. J., Campana, S., Chambers, K. C., Chen, T.-W., Della Valle, M., Dennefeld, M., Elias-Rosa, N., Galbany, L., Galindo-Guil, F. J., Gromadzki, M., Hiramatsu, D., Inserra, C., Leloudas, G., Müller-Bravo, T. E., Nicholl, M., Reguitti, A., Shahbandeh, M., Smartt, S. J., Tartaglia, L., Young, D. R. A long life of excess: The interacting transient SN 2017hcc. Astronomy & Astrophysics, 2023; volume 669, A51.

II Moran, S., Kotak, R., Fraser, M., Pastorello, A., Cai, Y.-Z., Valerin, G., Mattila, S., Cappellaro, E., Kravtsov, T., Gutiérrez, C. P., Elias-Rosa, N., Reguitti, A., Lundqvist, P., Filippenko, A. V., Brink, T. G. and Wang, X.-F. Red eminence: the intermediate-luminosity red transient AT 2022fnm. Astronomy & Astrophysics, 2024; volume 688, A161.

III Fraser, M., Moran, S., Kotak, R., Benetti, S., Jonker, P., Levan, A., Kuncarayakti, H., Lyman, J., Moriya, T., Pastorello, A., Smartt, S., Tucker, B., Wyrzykowski, L. Going nowhere fast: an ultra-stripped supernova with a large velocity offset from its host. To be submitted to Astronomy & Astrophysics, 2025.

1 Introduction

Transient astronomical phenomena (transients) are objects that appear in the sky and then disappear or fade away, lasting between milliseconds and years. They include asteroids and comets, as well as high-energy events such as supernovae (SNe) and tidal-disruption events (TDEs).

In the current era transients are typically detected by wide-field surveys such as the Asteroid Terrestrial-impact Last Alert System (ATLAS, Tonry et al. 2018; Smith et al. 2020), the Zwicky Transient Facility (ZTF, Bellm et al. 2019), the Gravitational-Wave Optical Transient Observer (GOTO, Gompertz et al. 2020; Steeghs et al. 2022) and the All-Sky Automated Survey for Supernovae (ASAS-SN, Shappee et al. 2014; Kochanek et al. 2017).

An overview of the parameter space of transient phenomena is offered in Fig. 1, with a plot of timescale versus peak optical luminosity, displaying their variation. In this thesis I will only focus on a small subset of the objects in the diagram, namely interacting core-collapse SNe (CCSNe), Ca-dominated SNe[1], ultrastripped SNe, TDEs, intermediate-luminosity red transients (ILRTs) and luminous red novae (LRNe). SNe are typically divided into two primary groupings: type I (hydrogen-poor SNe) and type II (hydrogen-rich SNe) (Minkowski, 1941). Further division takes place in accordance with additional spectroscopic and photometric observational features. The so-called "gap transients" occupy the luminosity range between core-collapse SNe, discussed in Section 1.3, and classical novae. The gap transients are a diverse group, with various physical origins, but they display some overlap in terms of duration and luminosity. They include the aforementioned ILRTs and LRNe, weak explosions within dense CSM, both of which will be further discussed in Chapter 3, as well as the Ca-dominated SNe, to be discussed in Chapter 4.

Transients are not studied merely for their own sake: many are connected to the formation of compact objects and are a key source of nucleosynthesis in the universe, chemically enriching the interstellar medium (Thielemann et al., 2011). Additionally, some can be used as cosmological distance indicators (Kirshner and Kwan, 1974). Transients can also be used to provide indirect evidence about the nature of high-redshift stars (Tanvir et al., 2009).

[1] commonly referred to as "calcium-rich SNe"

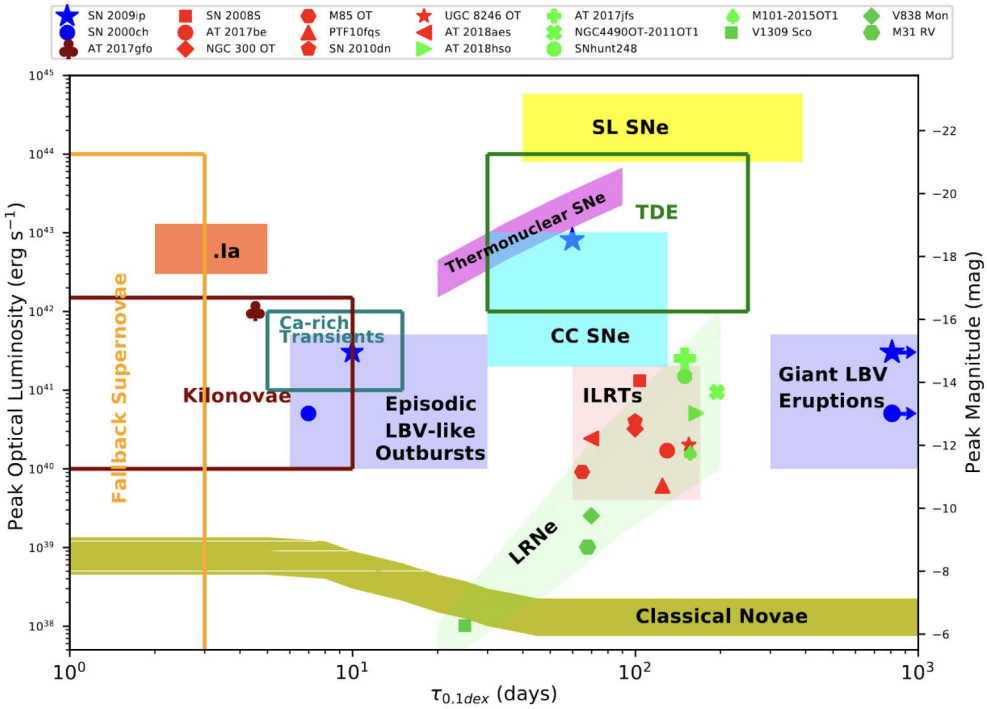

Figure 1. Diagram showing the parameter space of transient astrophysical phenomena. The time for the luminosity to decrease by 0.1 dex is shown on the x axis and the peak optical luminosity is shown on the y axis. Only some of the categories shown will be addressed in this thesis. Source: Cai et al. (2022a).

1.1 Stellar Evolution

In Fig. 2, I present the Hertzsprung-Russell diagram, which shows the relation between the luminosity of stars and their temperatures, where the luminosity can be expressed as,

$$L = 4\pi R^2 \sigma T^4 \tag{1}$$

where σ is the Stefan-Boltzmann constant, R is the stellar radius, and T is the effective temperature. The Hertzsprung-Russell diagram groups stars into different spectral classes depending on their temperatures. It is clear that in plotting the stars we observe on this diagram, a structure appears. The structure is indicative of the various phases of stellar evolution. In particular, we can see a roughly diagonal structure extending from near the upper left (hot and luminous) to the bottom right (cool and faint). This is the main sequence, the largest population of stars; it is the area on the HR diagram occupied by stars through most of their lives, extending from the point at which they initially begin nuclear fusion until approximately 10% of the original hydrogen content of the star has been converted to helium (Hansen et al., 2004; Carroll and Ostlie, 2017). Stars are often referred to in terms of the zero-age

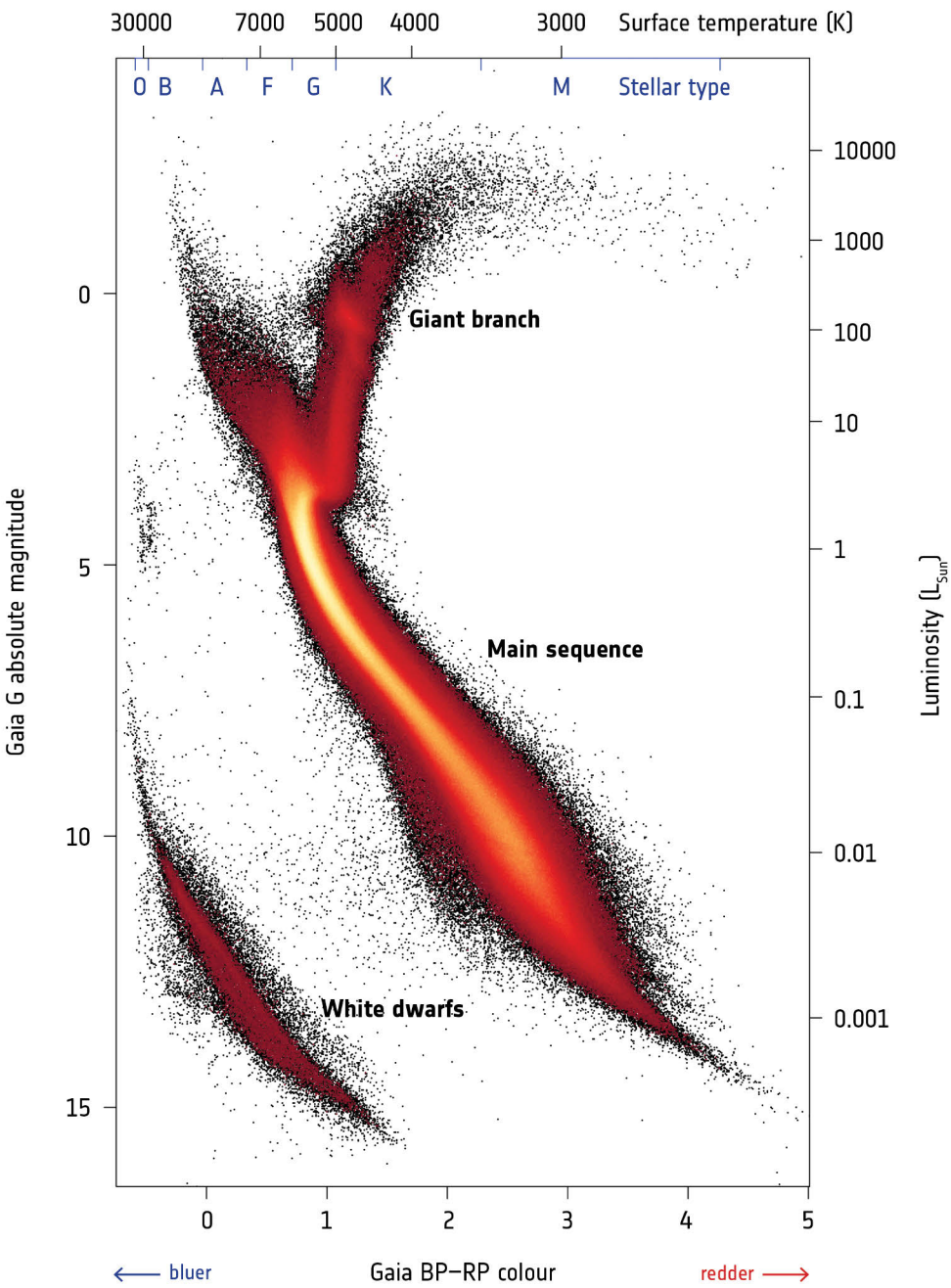

Figure 2. The Hertzsprung-Russell diagram from Gaia DR2, a plot of stars by their luminosity or absolute magnitude against their colour or effective surface temperature. Adapted from ESA/Gaia/DPAC original (CC BY-SA 3.0 IGO).

main-sequence (ZAMS) mass, which is their mass when they first enter the main sequence, that is, when the fusion of hydrogen in the stellar core becomes the primary source of energy (Kippenhahn et al., 2013).

The more massive the star, the less time it spends on the main sequence, and a star's position on the main sequence is governed by its mass, M, which is coupled to its luminosity, L, by the mass-luminosity relation,

$$L = M^a \tag{2}$$

where the exponent a varies depending on the stellar mass (Kuiper, 1938). Taking the mass-luminosity relation and comparing the energy released from the nuclear fusion of 10% of a star's hydrogen content with the main-sequence luminosity allows us to estimate the time a star will spend on the main sequence (Hansen et al., 2004),

$$t_{MS} \approx 10^{10}(\frac{M_\odot}{M})^{a-1} \text{ years} \tag{3}$$

As such, the Sun itself is expected to spend approximately 10^{10} years on the main sequence. Once a star ceases to fuse hydrogen in its core, it begins to evolve off the main sequence, and its mass will determine whether it becomes a supergiant, a red giant or a white dwarf (WD) (Karakas, 2017). With the cessation of the fusion of hydrogen in the core, the star contracts, heating the core and leading to sufficiently high temperatures to initiate the fusion of helium (Karakas, 2017). In smaller stars we instead get contraction until electron-degeneracy pressure re-establishes hydrostatic equilibrium, where the outward force due to the radiation pressure is balanced with the inward gravitational force,

$$\frac{dP}{dr} = -\frac{GM(r)\rho}{r^2} \tag{4}$$

where r is the radius, G is the gravitational constant, $M(r)$ is the mass inside the radius r, $\rho(r)$ is the density and $P(r)$ is the pressure (Chandrasekhar, 1935; Karakas, 2017). Very low mass stars ($\lesssim$0.23 $M_\odot$, assuming solar metallicity) are fully convective and evolve into helium (He) WDs after they finish burning hydrogen (Adams and Laughlin, 1997; Kippenhahn et al., 2013). Low-mass stars ($\lesssim$8 $M_\odot$) ultimately become carbon-oxygen WDs, intermediate-mass stars ($\sim 8-10$ $M_\odot$) eventually generate oxygen-neon WD cores before undergoing collapse via electron capture (to be discussed further in Chapter 3), whilst massive stars ($\gtrsim$10 $M_\odot$) instead end their lives as CCSNe (which will be discussed in more detail in Section 1.3), leaving behind a neutron star (NS) or black hole (BH) (Nomoto, 1984; Wheeler et al., 1998; Adams and Laughlin, 1997; Karakas, 2017). Note that these terminal scenarios concern single stars, whilst binarity can affect the endpoints of stellar evolution in different manners (Nomoto, 1984). Though supergiants are a key phase in the evolution of

massive stars before core-collapse, they are exceedingly rare on a population level, as can be seen in Fig. 2.

As a massive star evolves and progressively burns heavier elements, it builds up a number of onion-like layers, with lighter elements on the outside (Hansen et al., 2004). This is because the core is denser and hotter, and so can fuse heavier elements than the outer layers (Hansen et al., 2004). The composition of a massive star immediately before core collapse can be seen in Fig. 3, but note that this omits the stellar wind extending beyond the surface of the star and any circumstellar material (CSM) lost earlier in the star's evolution (Sieverding et al., 2021). More massive stars have denser, hotter cores and so nuclear fusion takes place more rapidly, exhausting their fuel at a higher rate and, as such, they move off the main sequence more quickly (Adams and Laughlin, 1997).

1.2 Mass Loss

The effects of mass loss on stellar evolution can be profound, so it is important to address the topic. In fact, massive stars often experience enhanced mass loss in the months to centuries prior to a SN explosion, which can have important effects on the photometric and spectroscopic evolution of the SNe (Fraser, 2020). Mass loss can be wind-driven, but it can also result from binary interaction (Smith, 2014). Wind-driven mass loss can itself be line-driven or continuum-driven (Owocki and van Marle, 2008). The mass-loss rate, $\dot{M}$, in the case of wind-driven mass loss with a steady wind can be described by the following equations,

$$\dot{M} \propto \frac{LR}{GM} \tag{5}$$

$$\dot{M} = 4\pi R^2 \rho_w \nu_w \tag{6}$$

where L is the luminosity, R is the stellar radius, G is the gravitational constant, M is the stellar mass, ρ_w is the wind density and ν_w is the wind velocity (Reimers, 1975; Blinnikov, 2017).

Metallicity has a profound effect on mass loss (Maeder and Meynet, 2000; Heger et al., 2003). So-called line-driven mass loss is metallicity dependent: in this kind of mass loss, radiation is absorbed and scattered by metals in the stellar atmosphere, and the resultant momentum transfer leads to gas being unbound from the star and lost (Lucy and Solomon, 1970). A somewhat simplified view is that line-driven mass loss M_{ld} scales as follows,

$$M_{ld} \propto Z^{0.5} \tag{7}$$

where Z is the metallicity (Nugis and Lamers, 2000). In reality, stellar winds are not homogeneous, the picture being complicated by the "clumpiness" of the wind; however, models that take such inhomogeneities into account produce results comparable to the simpler models (Smith, 2014).

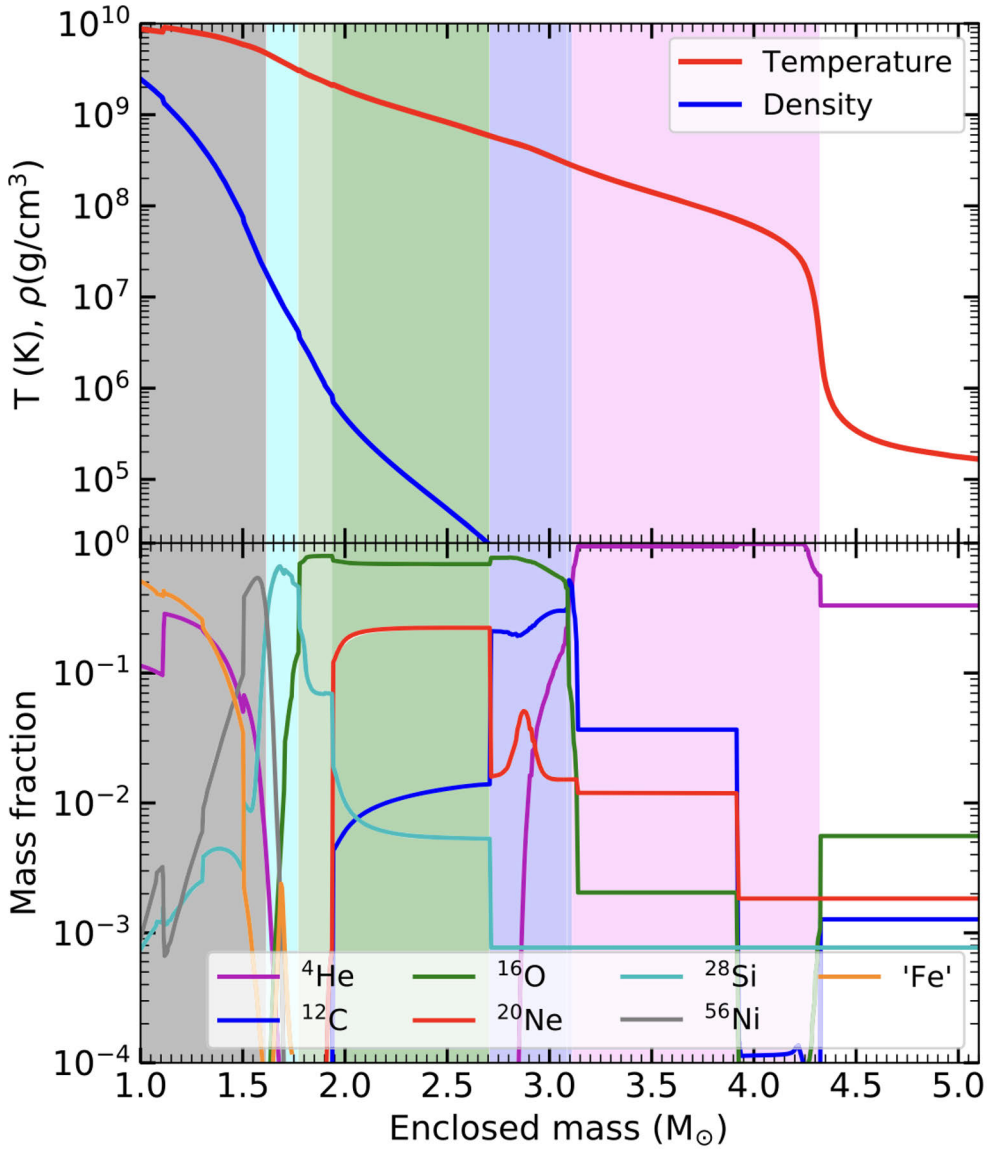

Figure 3. Stellar profile of a 15 $M_\odot$ star at core collapse. The upper panel shows the temperature and density profile of the star, whilst the lower panel shows its mass fraction for a number of important isotopes. Source: Sieverding et al. (2021).

Another form of mass loss is continuum-driven mass loss. In this case the winds are near the Eddington limit or even super-Eddington, meaning that the star is not in a state of hydrostatic equilibrium, the outward radiation pressure instead exceeding the inward gravitational pressure (Humphreys and Davidson, 1984; Owocki et al.,

2004). The Eddington limit is as follows,

$$L_{Edd} = \frac{4\pi c G M m_p}{\sigma_T} \tag{8}$$

where c is the speed of light in a vacuum, G is the gravitational constant, M is the stellar mass, m_p is the mass of the proton and σ_T is the cross section for Thomson scattering (Eddington, 1926; Branch and Wheeler, 2017). In such cases momentum is transferred from the radiation to the gas via electron scattering (Humphreys and Davidson, 1984; Owocki et al., 2004). Continuum-driven mass loss results in far greater mass loss than in line-driven cases (Owocki and van Marle, 2008). This kind of mass loss is believed to be the primary source of the giant eruptions in luminous blue variables (LBVs; massive unstable stars that undergo violent mass loss), though non-terminal hydrodynamic explosions may also account for some of these eruptions (Humphreys and Davidson, 1994; Owocki and van Marle, 2008; Smith and Owocki, 2006).

Binary interaction has large effects on stellar systems. Stellar rotation rates can be significantly altered by angular-momentum transfer: the star gaining mass will increase in angular momentum, the accretion leading to it being "spun up" by the other star, with the star losing mass correspondingly losing angular momentum (Langer et al., 2003; Langer, 2012). Extreme mass loss can result through Roche-lobe overflow, which will be discussed further in Chapter 3 (Ivanova et al., 2013). Furthermore, even the nuclear burning in a star can be impacted by binary interaction (Podsiadlowski et al., 2004).

1.3 Core-Collapse Supernovae

Sufficiently massive stars ($\gtrsim$10 $M_\odot$) end their lives as core-collapse SNe (see Fig. 4) once the mass of iron-group elements occupying the core exceeds the Chandrasekhar limit (approximately 1.44 $M_\odot$, Heger et al. 2003). This is because the fusion of elements heavier than those in the iron group is not energetically favourable (Janka et al., 2007). The iron core is formed, but energy is still lost in the form of neutrinos and through electron capture, the high densities leading to the capture of electrons by nuclei, reducing the electron degeneracy pressure, which had been the primary counterbalance to gravitational pressure (Janka et al., 2007). Additionally, the high temperatures also lead to photodisintegration, with gamma rays leading to the decay of the iron atoms through the emission of alpha particles and neutrons (Janka et al., 2007).

As a result of these processes, the core no longer produces sufficient radiation pressure to balance against gravitational pressure, and hydrostatic equilibrium is lost. The core contracts, decoupling from the other layers of the star and falling until it forms a proto-NS with a radius of approximately 30 km (Woosley and Janka, 2005).

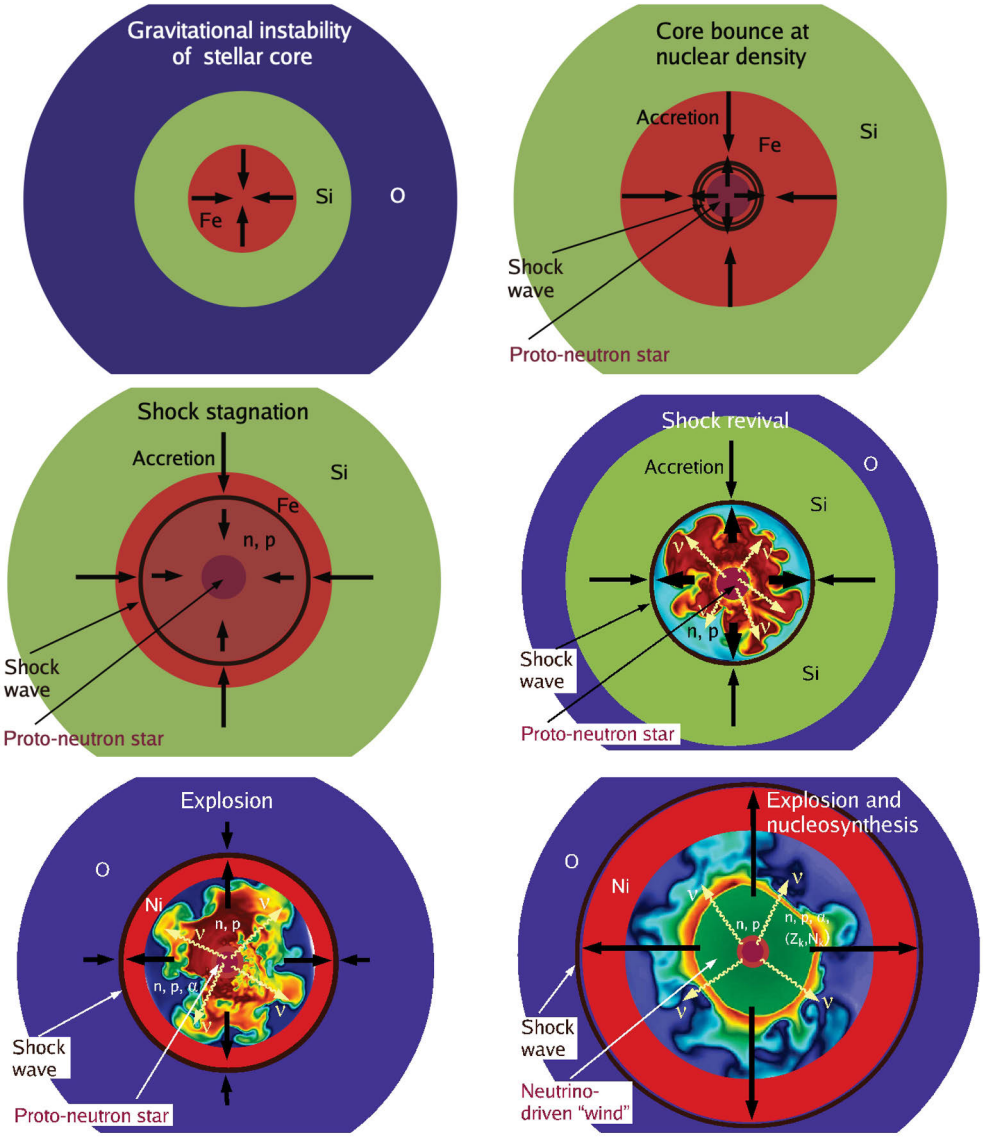

Figure 4. Representation of the steps from core collapse to SN explosion and nucleosynthesis. First the core develops a gravitational instability (top left), then we have the core bounce leading to the formation of the shock wave (top right). This is followed by the stalling of the shock wave (middle left), only for the shock wave to be reinvigorated (middle right). The explosion takes place (bottom left), with continuing formation of radioactive nickel as well as other kinds of nucleosynthesis in the neutrino-driven wind (bottom right). Source: Janka et al. (2012).

The outer core falls towards the proto-NS that the inner core has become, collides with it and is thrown outwards. The rebounding material collides with other material that is still falling inwards, and a shock wave is generated. However, the outwards

travelling shock wave is stalled before this material can be thrown off and if this stall is not counteracted, the proto-NS collapses to become a BH (Myra and Burrows, 1990).

Alternatively, it is thought that the shock wave may be re-energised by neutrino-driven convection with the proto-NS contracting to a radius of $\sim$10 km and becoming a NS whilst the explosion and concurrent nucleosynthesis (to be discussed below) proceed (Woosley and Janka, 2005; Janka et al., 2012). Though the precise details of the re-energising mechanism are not well understood, type II CCSNe release around $\sim 3\times10^{53}$ erg of gravitational binding energy in the form of neutrinos over the course of a few seconds during NS formation, which is two orders of magnitude higher than the kinetic energy of the explosion (Bionta et al., 1987; Hirata et al., 1987; Burrows, 2000).

1.3.1 Power sources

SNe can be powered in a number of ways, including the decay of radioactive elements, interaction with CSM, energy release from a magnetar (a NS powered by an extremely strong magnetic field) and fallback accretion onto a compact object resulting from the explosion (Mereghetti et al., 2015; Kaspi and Beloborodov, 2017; Kasen, 2017).

The initial electromagnetic emission from a SN results from shock breakout (Waxman and Katz, 2017). This occurs when the shock-wave optical depth falls to a point where photons can escape (Waxman and Katz, 2017). In the absence of CSM the process lasts less than an hour (and perhaps just seconds), but the presence of CSM can extend the duration to days (Waxman and Katz, 2017). The connection between shock-CSM interaction and luminosity will be discussed further in Chapter 2.

As seen in Fig. 4, ^{56}Ni is synthesised during the explosion process (Colgate and McKee, 1969; Arnett, 1982; Janka et al., 2012). This has a half-life of six days and decays to ^{56}Co, which has a half-life of 77 days, itself decaying to ^{56}Fe (Colgate and McKee, 1969). High-energy photons are generated during the decay processes and these photons deposit energy in the envelope (Colgate and McKee, 1969; Podsiadlowski, 2017).

1.3.2 Nucleosynthesis

The importance of CCSNe to nucleosynthesis was first brought to light by Burbidge et al. (1957) in the so-called "B^{2}FH paper" (following the initials of the authors). The nuclear burning process in the progenitor star generates progressively heavier elements. The SN explosion itself can generate yet heavier elements by means of the rapid neutron-capture process (r-process). The r-process is the primary process for

the generation of nuclei heavier than iron and is solely responsible for the production of elements heavier than lead and bismuth (Thielemann et al., 2011, 2017). The r-process involves the capture of neutrons by nuclei with sufficient rapidity that consecutive neutrons are captured before radioactive decay can take place (Thielemann et al., 2011). In order for the process to occur, there must be far more neutrons than seed nuclei (Thielemann et al., 2011).

The precise location in the SN where r-process nucleosynthesis actually occurs remains unclear, though suggestions include a high-entropy neutrino-rich wind and jets (Wheeler et al., 1998; Thielemann et al., 2011). Solar abundances of r-process elements can be well reproduced in simulations of nucleosynthesis in high-entropy neutrino winds (see Fig. 5; Kratz et al. 2014). Nevertheless, it is unclear whether such entropies can be achieved in actual core-collapse scenarios, though electron-capture SNe, to be discussed in Chapter 3, may be promising for the nucleosynthesis of elements up to europium (Thielemann et al., 2017).

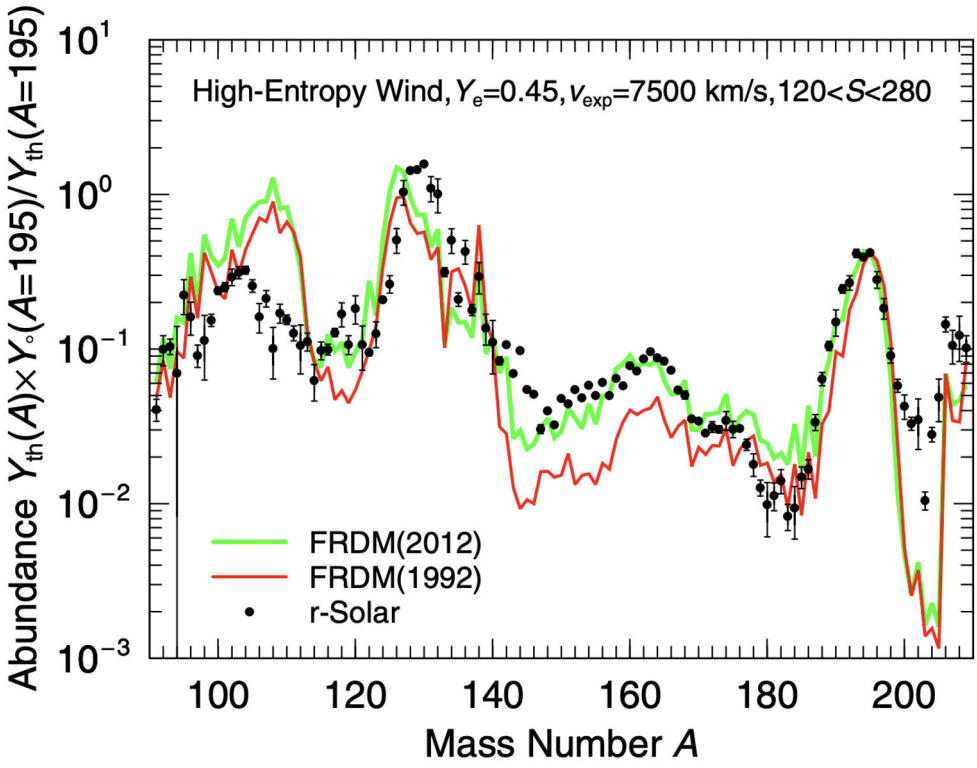

Figure 5. Plot of actual solar abundances of r-process elements compared with abundances generated in simulations of nucleosynthesis in high-entropy winds. FRDM(1992) and FRDM(2012) represent calculations based on two different nuclear-structure databases. Y_e is the electron fraction of the wind, v_{exp} is its expansion velocity and S is the radiation entropy in units of $k_B/baryon$. Source: Kratz et al. (2014).

1.3.3 The P-Cygni profile

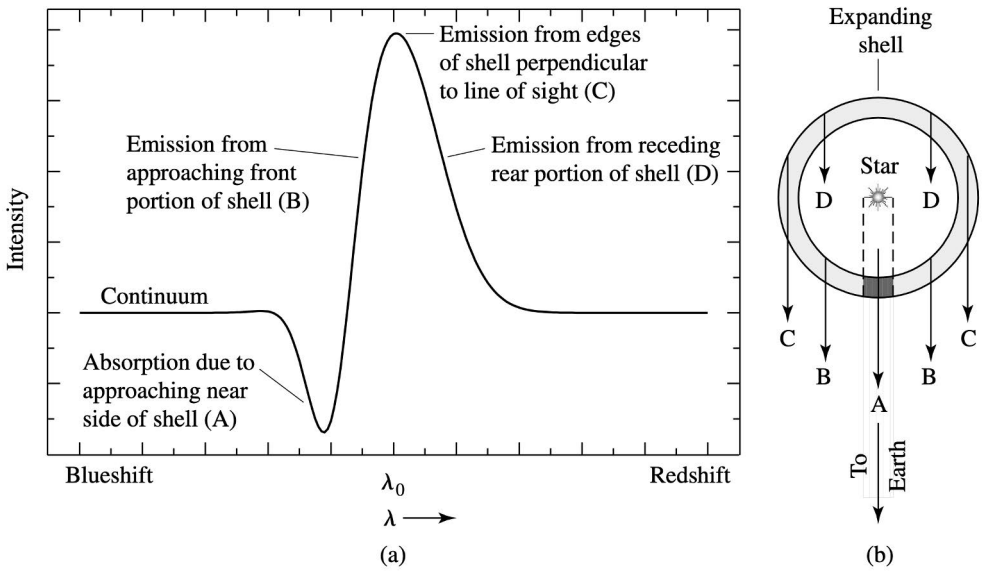

Figure 6. Left: P-Cygni profile showing the blueshifted absorption from the portion of the shell approaching the observer and the emission from the other portions. Right: a physical representation of the different regions of emission and absorption in the shell, with labels corresponding to the left part of the figure. Source: Carroll and Ostlie (2017).

A key observational feature observed in certain CCSNe is the P-Cygni profile (see Fig. 6), a composite spectral feature where both emission and blueshifted absorption are seen (Kirshner et al., 1973). The feature is named after the LBV P Cygni, which displays the prototypical example of the feature, the profile being visible in almost all the spectral lines of the star (Israelian and de Groot, 1999; Humphreys and Davidson, 1994; Kotak and Vink, 2006).

The absorption arises from the continuum passing through the cooler low-density gaseous envelope moving towards the observer, whilst the emission instead originates from hot diffuse gas with a component moving perpendicular to the line of sight (Lamers and Cassinelli, 1999; Carroll and Ostlie, 2017). SNe IIn, to be discussed in Chapter 2), are a subgroup of type II (i.e. hydrogen-rich) SNe, and display narrow ($< 1{,}000\,\mathrm{km\ s^{-1}}$) hydrogen emission lines in their spectra owing to CSM interaction (Schlegel, 1990). P-Cygni features in Hα, common in type II SNe, are sometimes observed in SNe IIn, though the greater and more enduring the CSM interaction, the less likely that such features will be seen as the photosphere will be concealed (Chugai et al., 2004; Smith, 2017). The superluminous (peak absolute bolometric magnitude < -21) type IIn SN 2006gy, for example, which peaked at least -21.8 in R band, showed a P-Cygni profile with outflow velocities of $-130\,\mathrm{km\ s^{-1}}$ in the trough and $-260\,\mathrm{km\ s^{-1}}$ at the blue edge, likely associated with dense unshocked

CSM (Chomiuk et al., 2011; Smith, 2017).

1.3.4 Dust

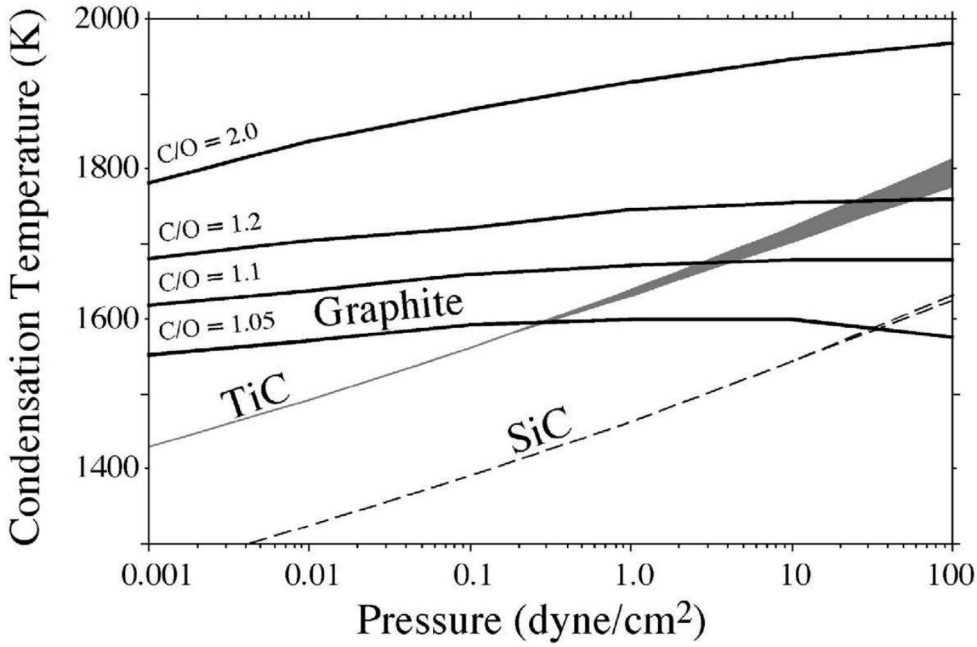

Figure 7. Condensation temperatures for graphite, silicon carbide (SiC) and titanium carbide (TiC) as a function of pressure. The effect of altering the C/O ratio is displayed in the case of graphite. Solar ratios for Ti/O and Si/O are assumed with a C/O ratio > 1.05. Source: Tielens et al. (2005).

Another indicator in observations of SNe that is important to consider is evidence of the presence of dust as this can give us insight into the environment of the SN and the evolutionary history of the progenitor star. Depending on the conditions of the explosion, SNe dust can be pre-existing or newly formed. There can be pre-existing dust from the interstellar medium or the progenitor star as well as dust condensation in SN ejecta (Hoyle and Wickramasinghe, 1962; Lucy et al., 1989; Kotak et al., 2009).

When the temperature of an element in the ejecta falls below its sublimation temperature, then dust condensation can take place (Tielens et al., 2005). The precise sublimation temperature depends on the kind of dust, the gas pressure and the C/O ratio, as is illustrated in Fig. 7 (Lodders and Fegley, 1995; Tielens et al., 2005). Dust can also form in the cool or cold dense shell (CDS, to be discussed in Chapter 2) that forms at the interface between the ejecta and CSM in interacting SNe (Matsuura, 2017). Type IIn SNe, to be discussed further in Chapter 2 are significantly over-represented (between around five and 20 times) when it comes to SNe presenting

late-time near-infrared excesses, indicative of the presence of warm dust (Fox et al., 2011; Eldridge et al., 2013; Li and Morozova, 2022).

Another factor to consider is pre-existing dust from the host galaxy itself, which can obscure SNe, preventing them from being detected in the first place (Mattila et al., 2012). Approximately 19% of SNe in the local universe are undetected at optical wavelengths owing to high levels of extinction from dust, and this rises to 38% at a redshift of $\sim$1.2 (Mattila et al., 2012).

Photometry allows us to determine the amount of energy radiated by an event as well as the colour and photospheric temperature and radius evolution (Dessart et al., 2022). Light curves also reflect radioactive-nickel yields and ejecta properties (Dessart et al., 2022). Spectroscopy gives insight into the chemical composition of transient events whilst also allowing us to constrain their geometry both by means of the velocities determined from emission and absorption lines, as well as by probing asymmetries along the line of sight (Dopita and Tuohy, 1984; Leonard et al., 2000).

Considering these data together, we can start to build a clearer picture of the formation of NSs and BHs and gain insight into the aforementioned nucleosynthesis and dust production. For example, photometrically, dust formation will lead to a near-infrared excess (i.e. more emission at near-infrared wavelengths than would be expected, given the blackbody temperature) and a change in the decline rate of the light curve (Lucy et al., 1989; Fassia et al., 2000). Spectroscopically, dust formation can reveal itself by the apparent blueshifting of spectral emission lines, the redder parts being obscured by the dust (Lucy et al., 1989; Gehrz and Ney, 1990; Wooden et al., 1993). We can also develop a better understanding of Galactic structure and, ultimately, cosmology.

1.4 Layout of the Rest of the Thesis

In Chapter 2 I discuss classical SNe IIn (iron core-collapse SNe within hydrogen-rich CSM) and in Chapter 3 I describe weak explosions within dense circumstellar material, in particular LRNe and ILRTs. In Chapter 4 I give an overview of peculiar stripped-envelope SNe. In Chapter 5 I summarise the included papers and in Chapter 6 I address the future of the field and its challenges.

2 Classical Type IIn Supernovae: Iron Core-Collapse Supernovae within Hydrogen-Rich Circumstellar Material

As briefly addressed in Chapter 1, SNe IIn are a subgroup of type II (i.e. hydrogen-rich) SNe which display narrow ($< 1{,}000\,\mathrm{km\ s^{-1}}$) hydrogen emission lines in their spectra as a result of CSM interaction (Schlegel, 1990). There is a great deal of observational diversity in SNe IIn: they show a wide range of peak luminosities, and their lifetimes vary significantly (Smith, 2017). The details of this heterogeneity will be examined in the following subsections.

It should be noted that the precise delineation of SNe IIn can be somewhat unclear; there can be difficulty, for example, in disentangling SNe IIn and SNe Ia-CSM (Smith, 2017), as they appear spectroscopically similar. Many SNe Ia-CSM are thought to be thermonuclear SNe exploding into pre-existing CSM, hence their designation, but this is not clear in all cases (Smith, 2017). Additionally, from a certain perspective, SNe Ia-CSM could be considered to be a kind of SN IIn, as the IIn designation is purely observational and SNe Ia-CSM display the required narrow lines. Furthermore, any kind of SNe or even any kind of non-SN explosive outflow could, in theory, appear as a IIn if the environmental features were appropriate for the relevant narrow-line formation (Kotak et al., 2004; Smith, 2017). In this chapter I will focus primarily on iron core-collapse SNe within hydrogen-rich CSM, and I will address other phenomena that technically satisfy the classification criteria for SNe IIn (namely, narrow hydrogen lines) in Chapter 3, as they are fundamentally different. However, SNe IIn-P, which are another kind of event showing features of interaction, are briefly addressed at the end of this chapter, along with the presentation of some related preliminary data.

Estimates vary in the literature as to the precise rates of SNe IIn as a fraction of CCSNe found in the local universe, with values ranging from $2.4\% \pm 1.4\%$ (Eldridge et al. 2013) to $6.5\% \pm 2.5\%$ (Li et al. 2011), but these values are highly sensitive to the sample chosen, particularly given the overall rarity of SNe IIn (Cappellaro et al., 2015).

Many SNe IIn display near-infrared excesses owing to the presence of dust (Gerardy et al., 2002; Fox et al., 2011). Such excesses can be produced in multiple ways: for example, pre-existing dust grains can scatter light emitted by the SN, reprocessing

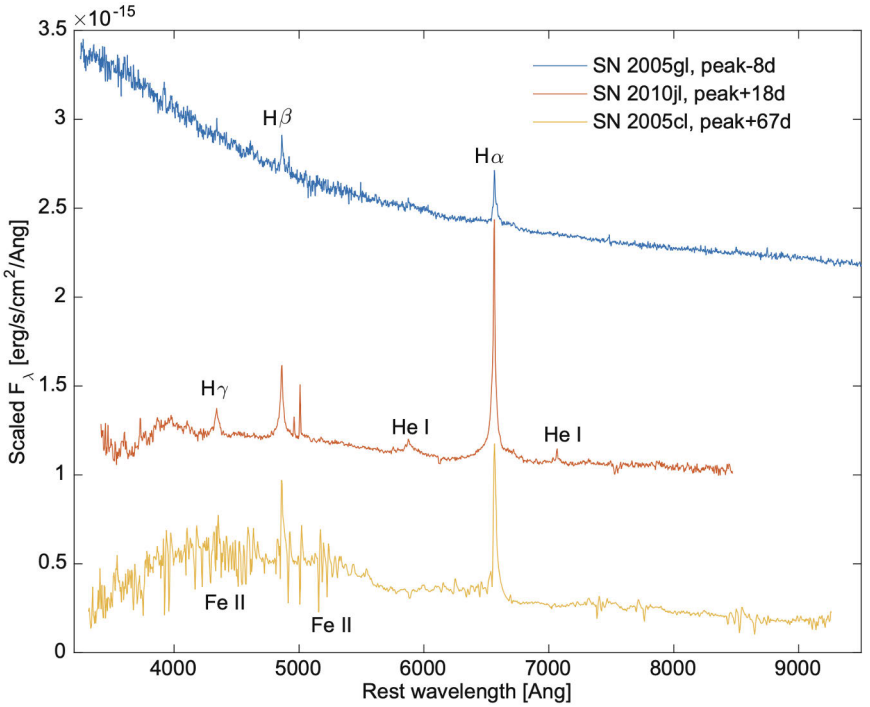

Figure 8. Three SN IIn spectra at pre-peak, post peak, and late times, showing the typical appearance of such objects at different points in their evolution. Note the presence of Balmer emission lines in each case. The pre-peak spectrum shows a blue continuum, the post-peak spectrum's Balmer and helium emission lines display extended wings, whilst a pseudo-continuum is present at late times. Source: Gal-Yam (2017).

it into redder wavelengths (Bode and Evans, 1979; Graham et al., 1983). It should be noted that the formation of dust can also result in an increasing near-infrared excess. Other signatures of dust formation are blueshifted line profiles and more rapid fading of the optical continuum (Lucy et al., 1989; Gehrz and Ney, 1990). There is a great deal of variation seen in the light curves of SNe IIn. Many display long-lasting and slowly evolving light curves, as in the case of SN 2010jl, which remained visible for years; however, others evolve far more quickly and can fade within months in the optical, as in the case of SN 1998S (Fassia et al., 2000; Ofek et al., 2019).

The peak magnitude of IIn light curves, as well as their overall shape, can give insight into the nature of the CSM in the environment of the SN. Indeed, many SNe IIn are very luminous owing to the CSM interaction that powers their light curves (Arcavi, 2017). SNe IIn peak luminosities cover a large range, spanning approximately six magnitudes (Arcavi, 2017). Additionally, pre-explosion outbursts, known as SN impostors, are seen in many SNe IIn, arising from non-terminal mass ejections (Reguitti et al., 2024).

We shall now address the nature of the spectra found in SNe IIn. As can be

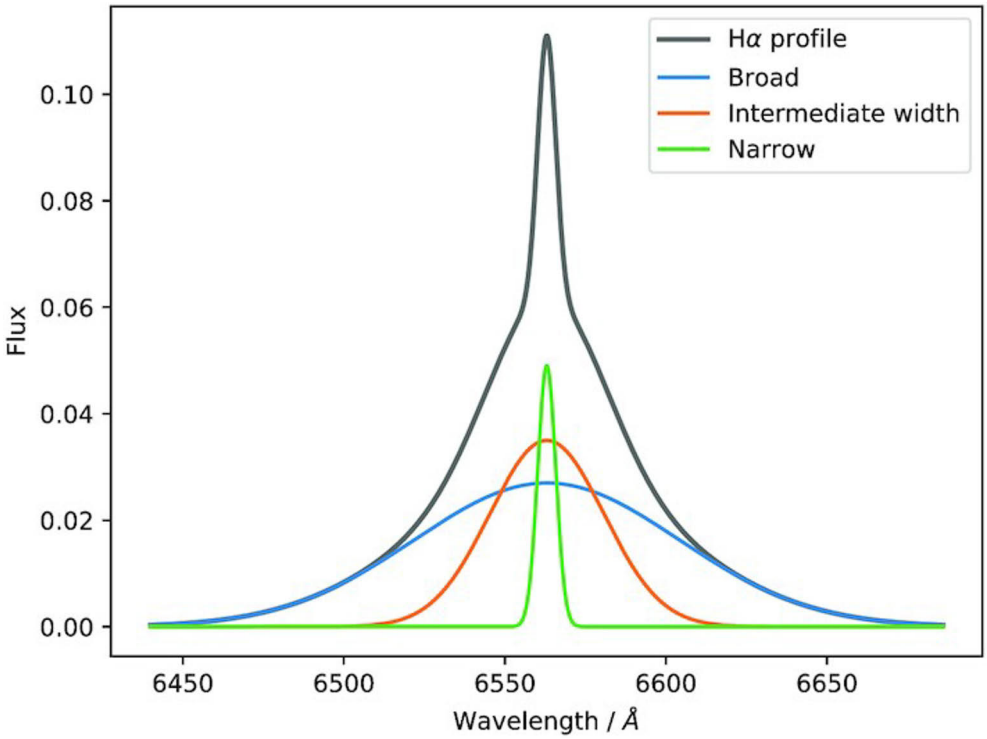

Figure 9. Three Gaussians fitted to the Hα profile. Showing the characteristic narrow line, but also a broad component arising from the fast-moving ejecta and an intermediate component with multiple possible origins including emission from the CDS or photons from interaction being scattered by thermal electrons, leading to broadening. Source: Ransome et al. (2021).

seen in Fig. 8, the spectra of SNe IIn show the presence of narrow ($< 1{,}000\,\mathrm{km\ s^{-1}}$) hydrogen lines by definition (Schlegel, 1990). These result from interaction, the ejecta impacting slow-moving massive and dense CSM and the ionisation of the CSM by the shock leading to the narrow emission (Chugai, 1997). Intermediate emission lines ($\sim 1{,}000$ to $2{,}000\,\mathrm{km\ s^{-1}}$) can arise from electron scattering or from emission from the CDS, whose formation is discussed below, whilst broad emission ($> 5{,}000\,\mathrm{km\ s^{-1}}$), when seen, instead arises from the fast-moving ejecta (see Fig. 9; Filippenko 1997; Ransome et al. 2021).

The nebular phase occurs when the photosphere recedes in mass space sufficiently to reveal the inner ejecta (Jerkstrand, 2017). In physical terms, this means that the density is low enough for the formation of forbidden lines (Jerkstrand, 2017; Inserra, 2019). Some SNe IIn, however, maintain CSM interaction in the long term, never reaching the nebular phase (Smith, 2017).

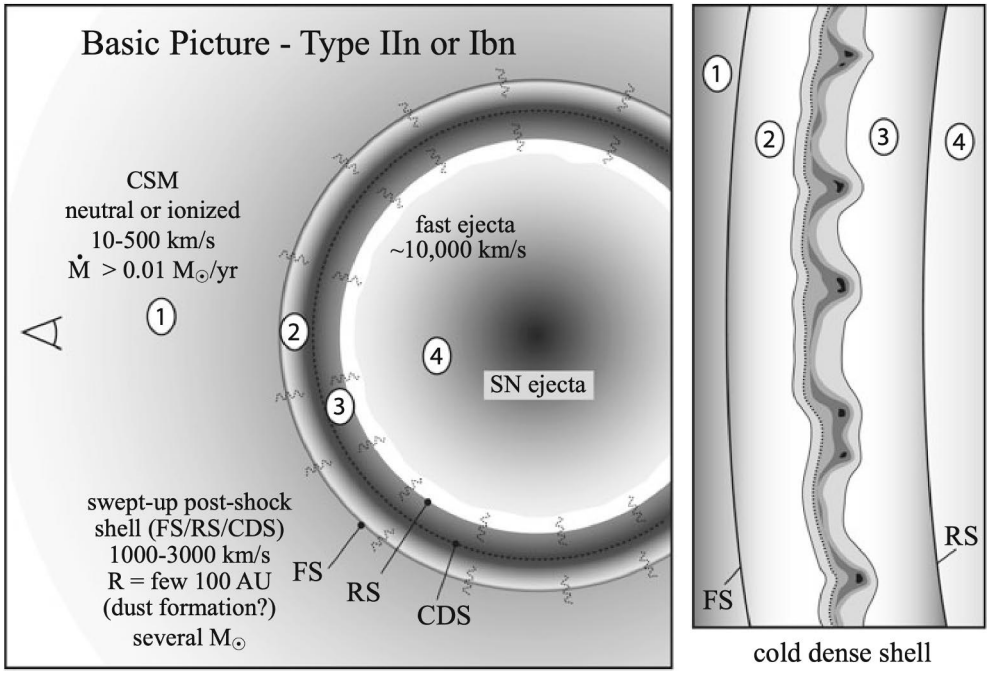

Figure 10. A simplified diagram of the basic structure of interacting SNe (i.e. SNe IIn and Ibn, where SNe Ibn, lacking hydrogen, instead show narrow helium lines). Zone 1 corresponds to the pre-shock CSM, zone 2 to the shocked CSM, zone 3 to the shocked ejecta and zone 4 to the freely expanding ejecta. FS - forward shock, RS - reverse shock. Source: Smith (2017).

2.1 Astrophysical Interpretation

SNe IIn constitute an observational class and a diverse one at that, but we can nevertheless attempt to provide a physical interpretation of these objects grounded in the observational properties we have already addressed.

Given the presence of narrow lines in the spectra of SNe IIn, we can infer the presence of an optically thin CSM that has been photoionised (Chugai, 1997). A simplified view of the structure of an interacting SN is offered in Fig. 10. In particular, we can see that a CDS forms between the forward and reverse shock of the SN. The CDS results from the cooling of the shocked CSM and the shocked ejecta that have been mixed owing to Rayleigh-Taylor instabilities, and its mass, greatly affected by the radius of the CSM, can be estimated as follows,

$$M_s \approx 2 \times 10^{-4} \left(\frac{R}{500\, M_\odot}\right)^2 \left(\frac{\nu_{sb}}{10^4\, km\ s^{-1}}\right)^{-1} \left(\frac{\kappa}{0.4\, cm^2 g^{-1}}\right)^{-1} M_\odot \qquad (9)$$

where R is the radius of the CSM, ν_{sb} is the velocity at shock breakout, and κ is the opacity of the material where the shell is formed (Chevalier, 1981; Blinnikov, 2017; Smith, 2017). The fast ejecta is travelling at approximately 10,000 km s^{-1}, whilst

the CSM is moving far more slowly, at roughly $10 - 500\,\mathrm{km\ s^{-1}}$(Smith, 2017). The cooler conditions of the CDS can allow for the formation of dust (Mattila et al., 2008).

The forward shock (see Fig. 10) will sweep mass up at the following rate,

$$\dot{M}_{fs} = 4\pi r^2 \rho_w \nu_{fs} \tag{10}$$

where ρ_w is the density of the wind and ν_{fs} is the velocity of the shock (Branch and Wheeler, 2017). Plugging that into Equation 1, we get the luminosity radiated away by the forward shock,

$$L_{fs} = \frac{\dot{M}_{fs}\nu_{fs}^2}{2} = 2\pi r^2 \rho_w \nu_{fs}^3 = \frac{\dot{M}_w \nu_{fs}^3}{2\nu_w} \tag{11}$$

where $\dot{M}_w$ is the wind mass-loss rate and ν_w is the velocity of the wind (Chevalier and Fransson, 2017; Branch and Wheeler, 2017). The luminosity radiated away by the reverse shock can be described similarly,

$$L_{rs} = \frac{\dot{M}_{rs}\nu_{rs}^2}{2} = 2\pi r^2 \rho_w \nu_{rs}^3 = \frac{\dot{M}_w \nu_{rs}^3}{2\nu_w} \tag{12}$$

where $\dot{M}_{rs}$ is the rate at which mass is swept up by the reverse shock and ν_{rs} is the velocity of the reverse shock (Chevalier and Fransson, 2017). This radiation can take a number of forms, including inverse Compton scattering in the shocked CSM, free-free emission in the forward and reverse-shocked regions and x-ray line emission from metals in the reverse-shocked ejecta (Branch and Wheeler, 2017). If the CSM is optically thick, then ionisation of the unshocked CSM by radiation from shock breakout or from x-rays from the region where interaction is taking place can lead to further emission (Branch and Wheeler, 2017).

2.1.1 Environments

Whilst most SNe II are believed to arise from red-supergiant progenitors, given the presence of massive CSM, SNe IIn must arise from stars with high mass-loss rates (Chevalier and Fransson, 1994). The mass-loss rates of the progenitor stars can be described as follows,

$$\dot{M} = \frac{2L\nu_{CSM}}{\nu_{CDS}^3} \tag{13}$$

where L is the luminosity of the SN, ν_{CSM} is the velocity of the CSM, and ν_{CDS} is the velocity of the CDS (Smith, 2017). The velocity of the CDS can be determined by measuring the intermediate lines in the spectra at late times and the velocity of the CSM can be determined by measuring the narrow lines (Smith, 2017).

Steady mass loss from massive stars is insufficient to provide CSM of the densities necessary to produce typical SNe IIn; such events instead require eruptive mass loss or episodic mass loss with only the former being sufficient in the case of superluminous SNe IIn (Smith, 2014). In particular, most kinds of SNe IIn are thought to originate from massive LBV-like stars, as the eruptive mass-loss of such stars can explain the high-density CSM apparent in such SNe, whilst steady stellar winds cannot (Kiewe et al., 2012; Smith, 2017). Furthermore, the mass loss must take place sufficiently close in time to the SN itself for the CSM to remain nearby or else interaction will not take place (Smith, 2014).

If there is dust present in the environment of the SN, then it can absorb incident light and re-emit it at longer wavelengths, which can result in the presence of a near-infrared excess in the light curve of the SN (Crotts, 1988). Depending on the location and geometry of the dust, light reflected from it may take a noticeably longer time to reach the Earth than light that has arrived directly, hence the term "light echo" (Couderc, 1939; Crotts, 1988).

Asymmetry of spectral lines can suggest the presence of dust, though such asymmetry can also result from asymmetric ejecta (Lucy et al., 1989; Taubenberger et al., 2009). Polarimetry can offer insight into asymmetric distributions of CSM as it traces asymmetry in the plane of the sky. This can be combined with spectroscopy, which traces asymmetry along the line of sight in order to build up a more complete picture of the layout of the CSM (Leonard et al., 2000).

2.2 Type IIn-P Supernovae

Another area for exploration is that of the so-called type IIn-P SNe, which throughout their evolution display the spectroscopic features of the shock interaction with dense CSM associated with IIn SNe, but also exhibit plateaus in their light curves, something characteristic of SNe IIP (Fraser, 2020; Mauerhan et al., 2013; Smith, 2013). They decline much more rapidly than would be expected from the decay of radioactive ^{56}Co, indicating low yields (Mauerhan et al., 2013). Members of this class include SN 1994W, SN 2005cl, SN 2009kn, SN 2011ht and SN 2020pvb, all of which featured outbursts before explosion, the material lost during which undoubtedly playing a role in the later interaction (Chugai et al., 2004; Kankare et al., 2012; Mauerhan et al., 2013; Li and Morozova, 2022; Elias-Rosa et al., 2024). It has also been proposed that SN 1054, the SN responsible for the formation of the Crab nebula, was a type IIn-P SN as it shows, for example, the telltale signs of having been a low-energy explosion with a low ^{56}Ni yield and also has the expected chemical abundances for such an event (Smith, 2013).

These events appear to be the result of relatively low-energy explosions ($\sim 10^{49}-10^{50}$ erg radiated electromagnetically), perhaps resulting from electron-capture SNe, which will be discussed in Chapter 3, or the core-collapse of massive stars with

significant fallback of metal-rich ejecta (Mauerhan et al., 2013; Smith, 2013). The continued disagreement as to the exact natures of the progenitors stresses the need for further observations and analysis of the precursor outbursts, which could shed more light on IIn-P origin scenarios (Elias-Rosa et al., 2024). Here I will present some preliminary unpublished data concerning one such object, SN 2020nub, for illustrative purposes.

2.2.1 SN 2020nub

SN 2020nub was first discovered by the ASAS-SN team at 02:38 on the 30th of June 2020 (MJD = 59030.11; (Stanek and Kochanek, 2020)). It was classified as a type IIn SN at redshift z = 0.017 by Dimitriadis et al. (2020) from the University of California, Santa Cruz on the 24th of July 2020 on the basis of observations taken with the LRIS instrument on the Keck I telescope. Here I show the light curve and spectral sequence of SN 2020nub, which demonstrate the features characteristic of type IIn-P SNe.

I obtained optical imaging from the ALFOSC instrument on the Nordic Optical Telescope (NOT) as part of the NUTS2 programme[1]. In addition, I also make use of observations taken as part of the Asteroid Terrestrial-impact Last Alert System (ATLAS) survey (Tonry et al., 2018; Smith et al., 2020). The first spectrum is the aforementioned publically available Keck+LRIS spectrum, which was obtained from the Transient Name Server[2]. I obtained the other spectra from NOT+ALFOSC as part of the NUTS2 programme.

The light curve, presented in Fig. 11, resembles that of a type IIP SN, displaying a plateau for approximately one month after peak before dropping sharply. At this point the SN went behind the Sun, becoming unobservable. By the time the SN returned, the rate of decline had significantly decreased, from approximately 0.3 mag per day in the o band at the end of season one to approximately 0.02 mag per day in the r band in season two. Both of these rates exceed the approximately 0.01 mag per day decline rate associated with the decay of radioactive ^{56}Co (Miller et al., 2010).

The spectra, presented in Fig. 12, span 69 days, from +28 d to +97 d. The +28 d spectrum shows a blue continuum, though the continuum gradually becomes redder later. The Balmer lines are evident throughout the evolution of the SN. A large change in the Balmer decrement (i.e. the ratio of the flux density of H_α to the flux density of H_β) is apparent over time. The decrement expected from recombination is 2.85 (Osterbrock, 1989). Higher values can result from the collisional excitation of H_β or from reddening due to dust as H_β is more attenuated by the presence of dust than is H_α, whilst lower values can result from the H_α-emitting region having a

[1] https://nuts.sn.ie/

[2] https://www.wis-tns.org/

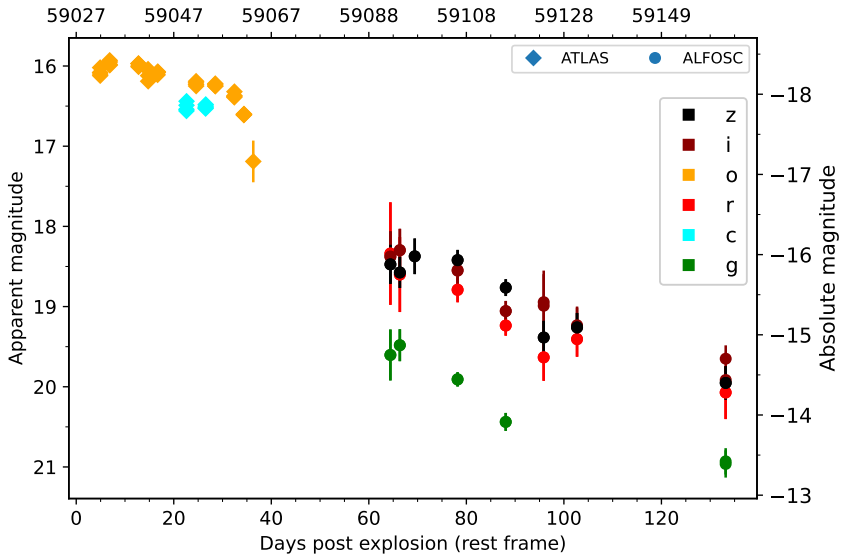

Figure 11. Multiband light curve of the type IIn-P SN 2020nub. The IIP-like plateau, characteristic of such events, is evident for about a month after peak before a steep drop in apparent magnitude occurs.

higher optical depth than the H_β-emitting region (Fraser et al., 2013; Levesque et al., 2014).

He I is visible in emission in the +28 d spectrum, but it is no longer obvious after this point until +51 d, following which it grows in prominence. The Ca II $\lambda\lambda\lambda$8498,8542,8662 triplet is evident from in the +28 d spectrum, but has greatly increased in prominence by the +66 d spectrum. O I is visible to the left of the near-infrared calcium triplet at all times, though it decreases in relative prominence as the SN evolves. The Fe II lines are clearly visible from the beginning up to the +86 d spectrum (inclusive), after which they are not readily visible above the noise.

The preliminary results shown in this elucidatory example highlight the characteristic plateau seen in such SNe, along with the narrow hydrogen lines also required for the IIn-P classification. Furthermore, the decline, in excess of that expected from radioactive ^{56}Co, is also typical of the class. Other objects displaying narrow Balmer lines, indicative of interaction, will be addressed in the next chapter.

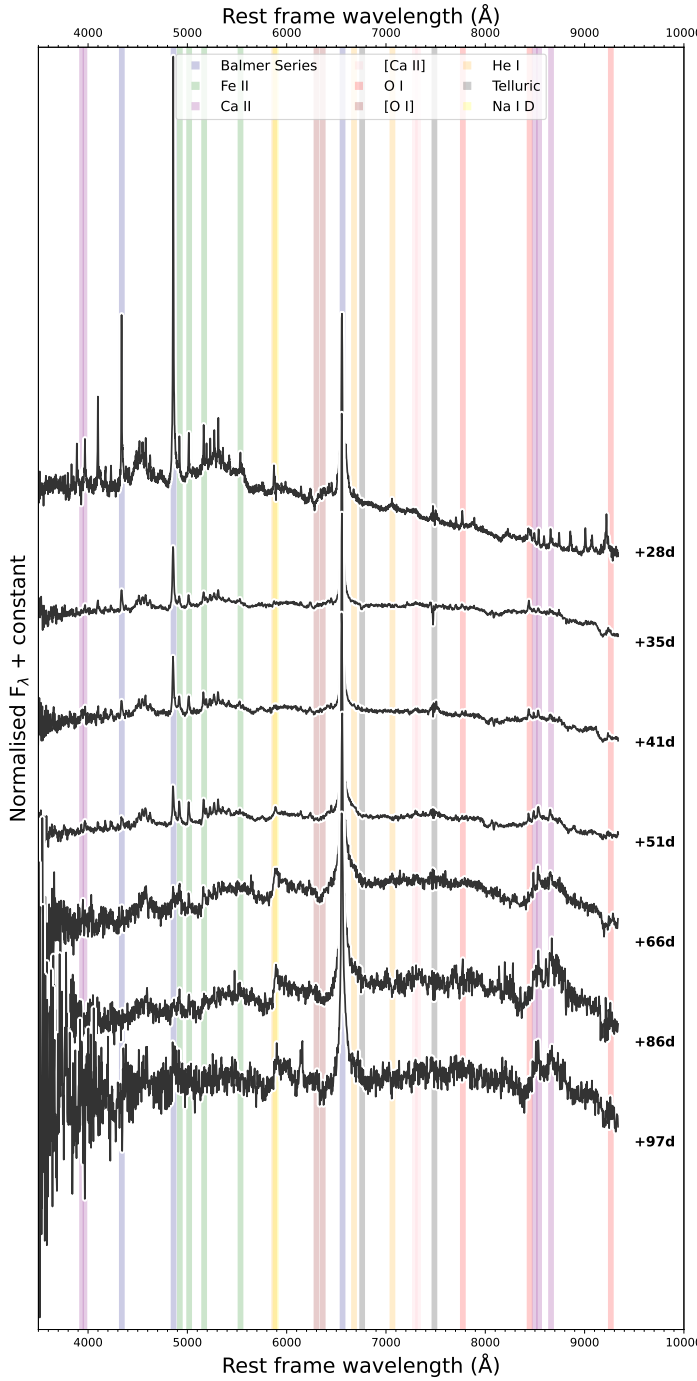

Figure 12. Spectral sequence of SN 2020nub. The flux densities of each spectrum have been normalised against the peak of Hα. A very large increase in the Balmer decrement (i.e. the ratio of the flux density of H_α to the flux density of H_β) is evident between the +28 d and +35 d spectra. The initial spectrum also shows a blue continuum not evident at later times.

3 Weak Explosions within Dense Circumstellar Material

In this chapter I will address particular kinds of weak explosions (i.e. events reaching a peak absolute magnitude of no more than around -15 mag) taking place within circumstellar material. This can encompass a broad range of event types, but only the kinds most relevant to my research will be treated here. The emphasis on the fact that these are weak explosions serves to differentiate these objects from the SNe IIn covered in Chapter 2.

3.1 Luminous Red Novae

LRNe display double-peaked light curves (see Fig. 13) with peak magnitudes covering a broad range of approximately -4 to -15 (Blagorodnova et al., 2017; Pastorello and Fraser, 2019; Pastorello et al., 2019). LRNe show a slow rise over months to years before a rapid increase in luminosity just before the first peak (Pastorello et al., 2023).

Certain binary stars spend a short period orbiting one another inside a shared envelope (Ivanova et al., 2013). The Roche lobe of a star in a binary system is the region around the star in which matter is gravitationally bound to it (Paczyński, 1971; Ivanova et al., 2013). The expansion of one of the stars or the decrease in orbital separation between the stars leads to Roche-lobe overflow, with mass transfer taking place from one of the stars, the donor, to the other star, the accretor (Paczyński, 1971; Ivanova et al., 2013). Should the accretor be unable to accrete all of the overflowing material from the donor star, then a common envelope will be formed and the drag generated as the stars move through this envelope will slow them, reducing their orbital separation even further over time (Paczynski, 1976; Ivanova et al., 2013). Eventually, the stars will either merge directly or eject the common envelope (Paczynski, 1976; Ivanova et al., 2013).

LRNe are generally believed to arise from stellar mergers and, indeed, display signatures of common-envelope ejection (Pastorello et al., 2019). The initial blue peak is often suggested to result from gas outflows or the cooling emission of the common envelope post ejection, whereas the later red peak results from hydrogen recombination, as in SNe IIP, or from radial heating from shock interaction (MacLeod et al., 2017; Metzger and Pejcha, 2017; Blagorodnova et al., 2021; Matsumoto and

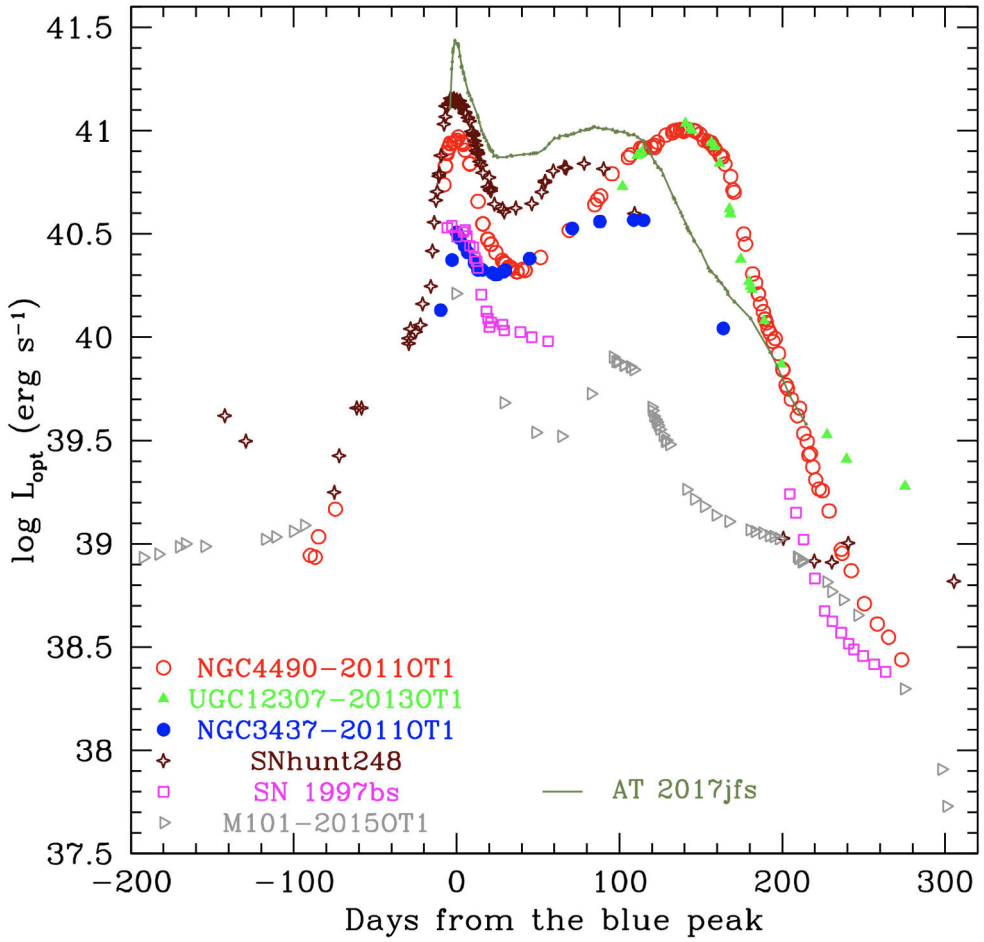

Figure 13. Pseudobolometric light curves of seven LRNe. All but SN 1997bs and UGC12307-20123OT1 were sufficiently well observed for the characteristic double peak to be seen. Source: Pastorello et al. (2019).

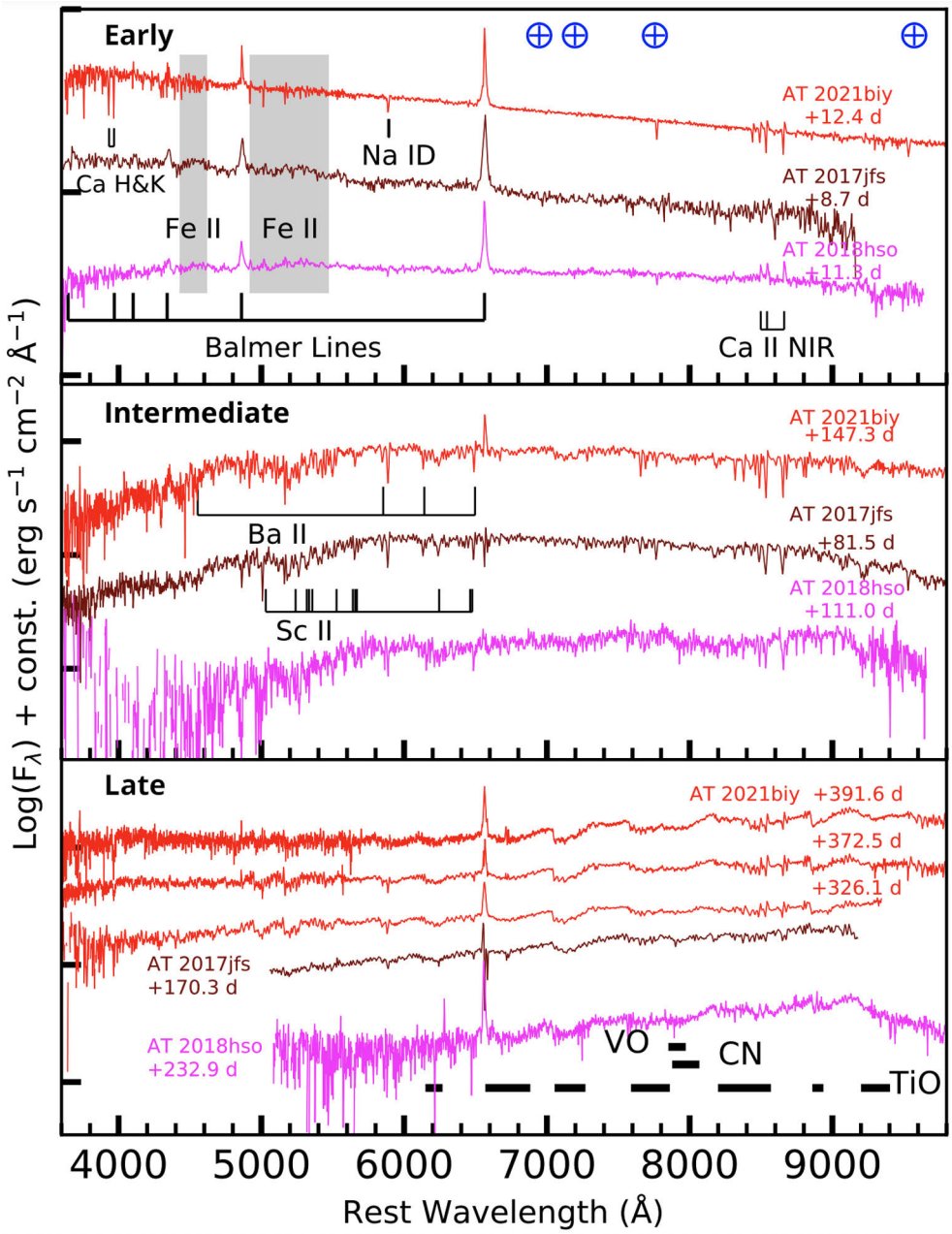

Figure 14. A series of LRNe spectra at early, intermediate and late times. The early spectra display the typical Balmer and Fe II emission lines. The forests of metal lines appear in the intermediate spectra whilst the late spectra show the characteristic molecular absorption bands. Adapted from Cai et al. (2022b).

Metzger, 2022).

The first, or "blue", peak in the light curve shows Balmer and Fe II lines in emission (see Fig. 14), reminiscent of SNe IIn (Cai et al., 2019, 2022b). Around the time of the second, or "red", peak in the light curve, the Balmer lines weaken, and a forest of metal lines in absorption appears (Pastorello et al., 2019). At late times LRNe have very red spectra that resemble those of M-type stars, with titanium monoxide and vanadium monoxide molecular absorption bands (Pastorello and Fraser, 2019).

The key to the classification of these events as stellar mergers came with observations of V1309 Scorpii. This event showed clear evidence of periodicity, with the luminosity evolving in a way consistent with a decreasing orbital distance resulting from binary inspiralling, with the period decreasing exponentially from an initially observed 1.4-day period (Tylenda et al., 2011). Additionally, the evolution of the light curve showed the two peaks characteristic of LRNe and the spectral properties typical of LRNe, such as a forest of metal absorption lines, were also present (Mason et al., 2010).

Mergers have a much higher rate of occurrence than SNe, with galactic stellar mergers of absolute magnitude $M_V = -3$ or greater occurring at a rate of approximately one every two to three years (Kochanek et al., 2014). Even events as luminous as V1309 Scorpii ($M_V \approx -7$ mag), can be expected about once every ten years (Kochanek et al., 2014). Mergers can be expected to greatly outnumber CCSNe: CCSNe require massive stars, but most massive stars are found in binaries and low-mass stars, which, owing to the initial mass function, greatly outnumber massive stars, can also be found in binaries, though the binary fraction decreases with decreasing mass (Salpeter, 1955; Chabrier, 2003; Stanway et al., 2020).

3.2 Intermediate-Luminosity Red Transients

ILRTs are another kind of gap transient, and they show a number of observational similarities with LRNe. Their peak absolute magnitudes are typically between -11.5 and -14.5, and their rises typically last approximately two weeks; however, the sample size of objects with a constrained rise time remains small, and variation is present (Cai et al., 2018, 2021; Stritzinger et al., 2020). After peak they tend to exhibit a plateau, resembling SNe IIP (Cai et al., 2021).

A key feature seen in ILRT spectra throughout their evolution is the [Ca II] $\lambda\lambda$7291,7323 doublet (see Fig. 15; Cai et al. 2021). The presence of the Ca II H&K lines and the Ca II λ8498,8542,8662 near-infrared triplet is also typical (Cai et al., 2021). The vast majority of stars with a ZAMS mass of $0.9 - 8\,\mathrm{M}_\odot$ pass through an asymptotic giant branch (AGB) stage (an evolutionary stage reached after the end of helium burning in the core) and ultimately end their lives as WDs (Karakas, 2017). $7.5 - 9.25\,\mathrm{M}_\odot$ is the mass range for super-AGB (sAGB) stars (Poelarends et al., 2008). Larger stars, up to about $40\,\mathrm{M}_\odot$, typically become red supergiants

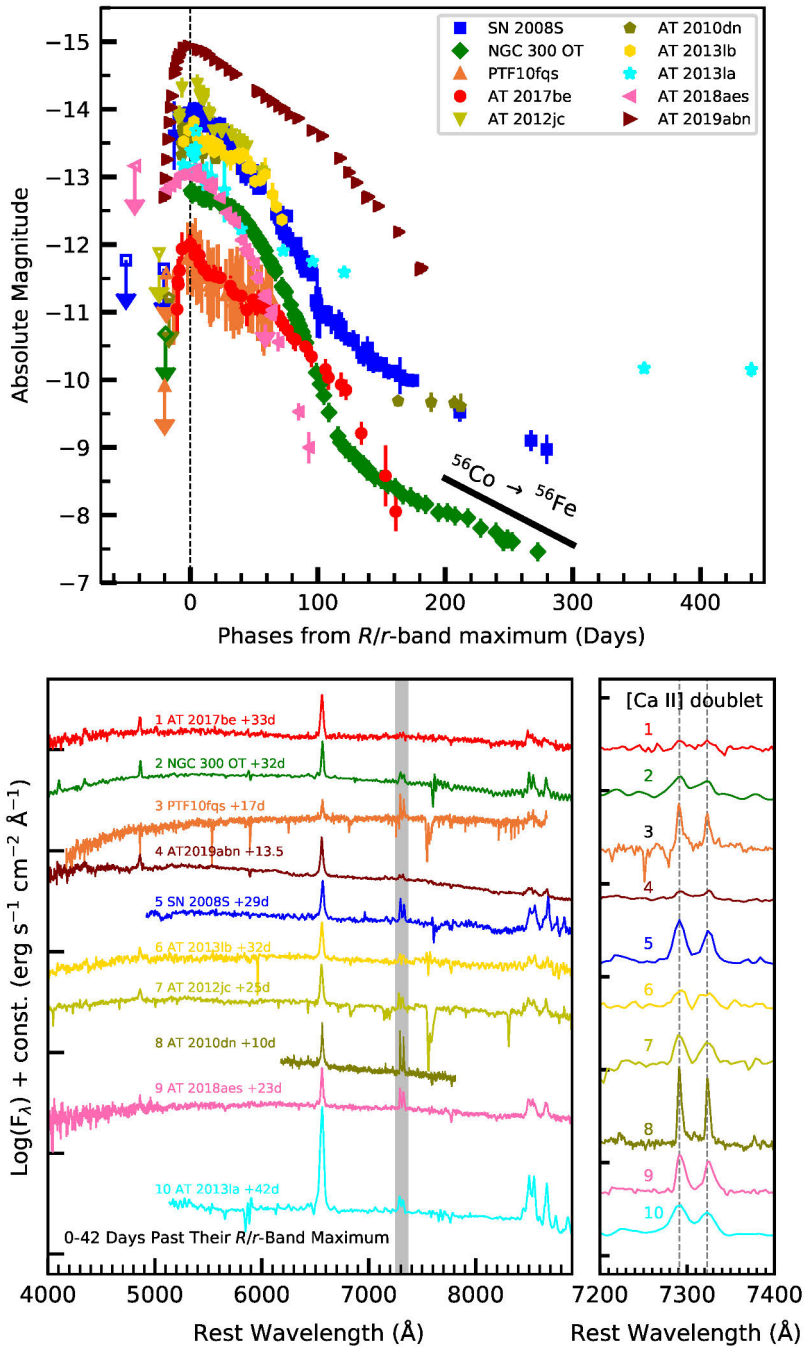

Figure 15. Sequence of ILRT light curves (upper panel) and spectra (lower panels). The typical light-curve rise times of approximately two weeks can be seen in the upper panel along with, in the case of most of the objects, the characteristic IIP-like plateau. The lower right panel shows a blown-up view of the characteristic [Ca II] $\lambda\lambda$7291,7323 doublet that is present throughout the evolution of ILRTs. Source: Cai et al. (2022a).

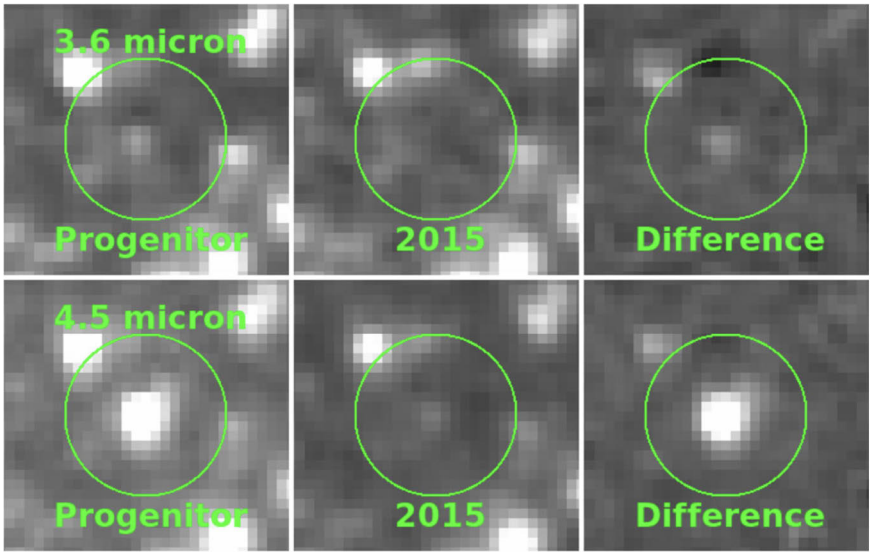

Figure 16. *Spitzer Space Telescope* images of the site of NGC 300 2008OT-1. The top row is in the 3.6-micron band and the bottom row is in the 4.5-micron band. The left column shows the site before explosion and the centre column after explosion, whilst the final column shows the difference between the two. The difference images illustrate that there is a significant decrease in brightness between the pre-explosion and post-explosion imagery, suggesting that this was a terminal event. Source: Adams et al. (2016).

(RSGs) before exploding as CCSNe (Groenewegen and Sloan, 2018; Humphreys et al., 2020).

Various scenarios have been suggested for the production of ILRTs, but the origin channel currently favoured is that of electron-capture SNe (ECSNe), terminal events arising from sAGB stars (Pumo et al., 2009; Thompson et al., 2009), and so I focus on that here. In particular, ECSNe are far more likely to form in binary systems than from single stars (Podsiadlowski et al., 2004). At the ends of the lives of stars with masses in the transitional zone between those of intermediate-mass stars and massive stars, a SN can take place, but through a different mechanism than core collapse (Nomoto, 1984; Wheeler et al., 1998). This transitional zone occupies a mass range between approximately $8-10\,M_{\odot}$; however, the precise range is sensitive to metallicity (Langer, 2012). Such stars form a degenerate oxygen-neon-magnesium core rather than an iron core (Wheeler et al., 1998). This core falls in a mass range of approximately $1.1-1.37\,M_{\odot}$. The lower limit is the point above which C burning can take place to lead to the formation of the oxygen-neon-magnesium core, and the upper limit is the point at which ignition of Ne would take place (Nomoto and Leung, 2017). The fusion of H and He in the shells leads to an increase in the mass of the core, which causes it to contract, ultimately leading to electron capture which leads to further contraction and, eventually, deflagration (Nomoto and Leung, 2017).

There is support for the notion that ILRTs may in fact be terminal: progenitors have been detected in the case of two ILRTs, SN 2008S and NGC 300 2008OT-1, with post-explosion imaging (see Fig. 16) having shown luminosities lower than those visible before the explosions (Adams et al., 2016). It should be noted that other potential origin pathways from ILRTs have been suggested in the literature. For example, it has been suggested that ILRTs are outbursts of stars of around 20 $M_{\odot}$ in dusty cocoons powered by super-Eddington winds (Smith et al., 2009). Another possibility is that ILRTs are instead powered by mass transfer from an AGB star to a main-sequence star (Kashi et al., 2010).

4 Fast-Evolving Transients

There are various kinds of fast-evolving transients (e.g. optical gamma-ray burst afterglows and fast blue optical transients; Fox et al. 2003; Fang et al. 2019), but here I am focusing on peculiar stripped-envelope SNe and tidal-disruption events (TDEs) as they have the greatest relevance to my own research.

4.1 Peculiar Stripped-Envelope Supernovae

Standard stripped-envelope SNe arise from stars that have lost their outer envelopes of hydrogen or of both hydrogen and helium through binary interaction or through the activity of intense stellar winds and, as such, they display no hydrogen in their spectra (Smith, 2014). Their light curves are traditionally taken to be powered by radioactive decay, though recently, a central-engine power source has been proposed (Rodriguez et al., 2024). In particular, I will focus on calcium-dominated SNe and ultrastripped SNe.

4.1.1 Calcium-dominated supernovae

Calcium-dominated SNe[1] are a form of gap transient, with peak absolute magnitudes falling between -15.5 to -16.5 in the R band (Kasliwal et al., 2012). They have been estimated to occur at a rate approximately $7\% \pm 5\%$ of that of type Ia SNe (Perets et al., 2010). They show rapid photometric evolution, with rise times of approximately two weeks, and large photospheric velocities ($\sim$ 6,000 to 10,000 km s^{-1}) (Kasliwal et al., 2012). They also swiftly move to the nebular phase, from around one to three months after explosion, and display intense calcium lines in their spectra (see Fig. 17), something central to their classification (Perets et al., 2010; Kasliwal et al., 2012).

Additionally, calcium-dominated SNe are notable for their tendency to have pronounced offsets from their host galaxies (Kasliwal et al., 2012; Lyman et al., 2016; Lunnan et al., 2017). Both thermonuclear SNe and CCSNe have been suggested as potential origin pathways for calcium-dominated SNe, but in either case non-

[1] These are commonly referred to as "calcium-rich SNe", but whilst their spectra are dominated by calcium lines that does not necessarily imply that there is a great deal of calcium present.

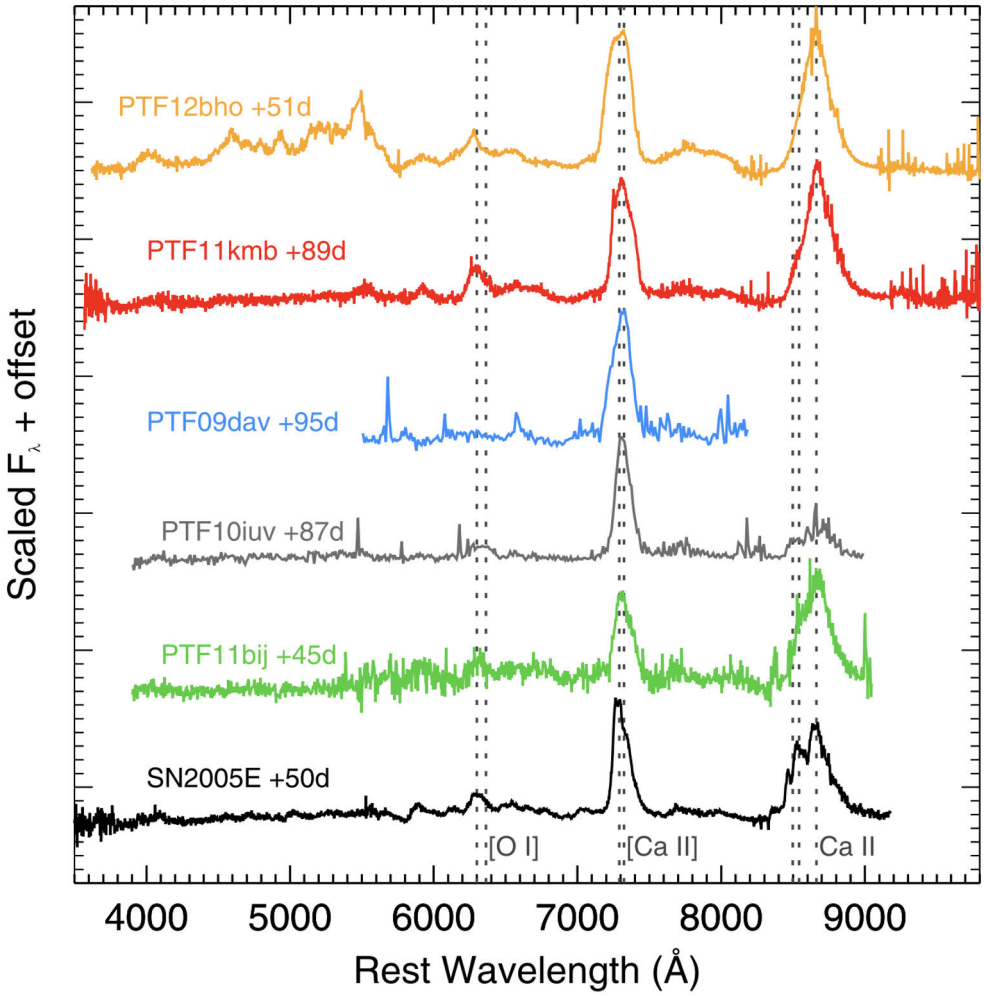

Figure 17. Nebular spectra of a selection of calcium-dominated SNe. The characteristic [Ca II] $\lambda\lambda$7291,7323 doublet is prominent as is the near-infrared Ca II λ8498,8542,8662 triplet. The highlighted [O I] emission is far weaker by comparison. Source: Lunnan et al. (2017).

standard channels would be required: for example, the explosion of a white-dwarf core, potentially with interaction between the shock and previously ejected material, or, in the case of a massive star, perhaps the fallback of ejecta onto the core resulting in the formation of a BH (Kasliwal et al., 2012).

4.1.2 Ultrastripped supernovae

Ultrastripped SNe (USSNe) are faint, with peak luminosities $< 10^{42}$ erg s^{-1}, and they fade quickly (Tauris et al., 2013, 2015). They display evidence of very low ejecta masses ($< 0.1\,M_\odot$) as a result of extensive stripping, and they produce cor-

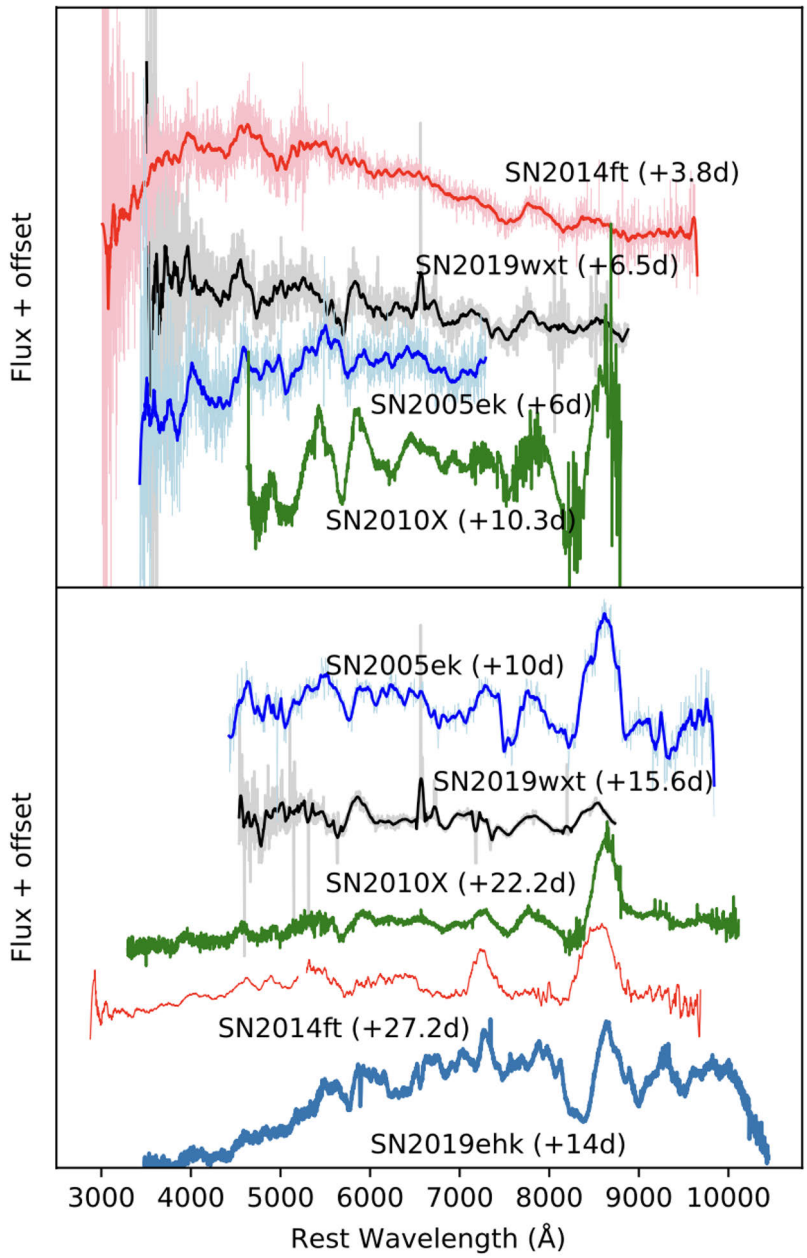

Figure 18. Comparison of a selection of USSNe at similar phases. The upper panel shows early phases, whilst those in the lower panel are later. The later spectra agree particularly well, being especially similar at their redder ends, though the near-infrared Ca II λ8498,8542,8662 triplet is weaker in the case of SN 2019wxt. Spectra with low S/N have been smoothed. Note that the identification of SN 2019ehk as an USSN is contested owing to the potential presence of hydrogen (Yao et al., 2020; Jacobson-Galán et al., 2020; De et al., 2021). Source: Agudo et al. (2023).

respondingly small masses of ^{56}Ni ($\sim 0.01\,M_\odot$; Tauris et al. 2013, 2015). Such intensive stripping is possible as their progenitors have compact companions whose small size permits the formation of tight binaries where stripping is enhanced (Tauris et al., 2013, 2015). Given their small ejecta masses, they evolve rapidly, typically rising to peak over the course of five to ten days (Tauris et al., 2013).

Close binary interaction can result in both iron CCSNe and ECSNe, with models suggesting that USSNe can arise from either (Tauris et al., 2015). In the case of close binaries resulting in iron CCSNe, large asymmetric kicks ($> 1{,}000\,\mathrm{km\ s^{-1}}$) can be expected (Scheck et al., 2006). The large kicks from the explosion would lead the stars to become runaway stars thrown away with large velocities (Tauris et al., 2015). On the other hand, ECSNe are expected to result in practically symmetric explosions and, hence, should produce minimal kicks (Podsiadlowski et al., 2004).

USSNe are typically thought to be CCSNe resulting from the explosion of bare $1.5\,M_\odot$ metal cores, which is at the lower end of what is possible in terms of mass (Tauris et al., 2015). The near-infrared Ca II λ8498,8542,8662 triplet is typically present in the spectra of USSNe at late times (see Fig. 18), and indeed comparisons between the observed spectra of calcium-dominated SNe and simulated spectra of USSNe suggest that these classes of events may be connected (Moriya et al., 2017; Nakaoka et al., 2021). USSNe offer one pathway for the formation of double-NS binaries, which can merge to produce kilonovae (the electromagnetic transients resulting from the merger of two NS or a NS and a BH; Tauris et al. 2015, 2017). Such mergers are detectable in the form of gravitational waves (distortions of spacetime produced by concentrations of mass or energy) by instruments such as the interferometers LIGO and Virgo and also optically, as in the case of the event AT 2017gfo (Barish, 1999; Metzger et al., 2010; Tauris et al., 2015; Abbott et al., 2017b).

4.2 Tidal-Disruption Events

TDEs are another kind of phenomenon that can produce fast-evolving optical transients. They are expected to occur at a rate of approximately 10^{-5} to 10^{-6} per galaxy per year, with the higher end of the range corresponding to active galaxies, though obscuration by dust can result in non-detection, especially at higher redshifts (Donley et al., 2002; Mattila et al., 2018).

A classical TDE occurs when a star ventures too close to a supermassive BH (SMBH) and becomes disrupted by the consequent tidal forces once they exceed the star's self-gravity (Hills, 1975). Almost half of the disrupted material will then escape on hyperbolic orbits, but the rest of the disrupted material will be circularised, forming an accretion disc (Rees, 1988; Gezari, 2021). This material will then be accreted onto the SMBH resulting in the production of a luminous flare of electromagnetic radiation, with the nature of the flare reflecting the structure of the ejected material and of the accretion disc formed (Rees, 1988; Arcavi et al., 2014; Komossa,

2015; Gezari, 2021). The physical details of the accretion process remain unclear (Gezari, 2021). It is also possible that the circularisation of the accretion disc proceeds slowly, in which case the luminosity must originate from another physical process, such as emission resulting from interaction from the collision of debris streams as they fall onto the black hole (Gezari, 2021).

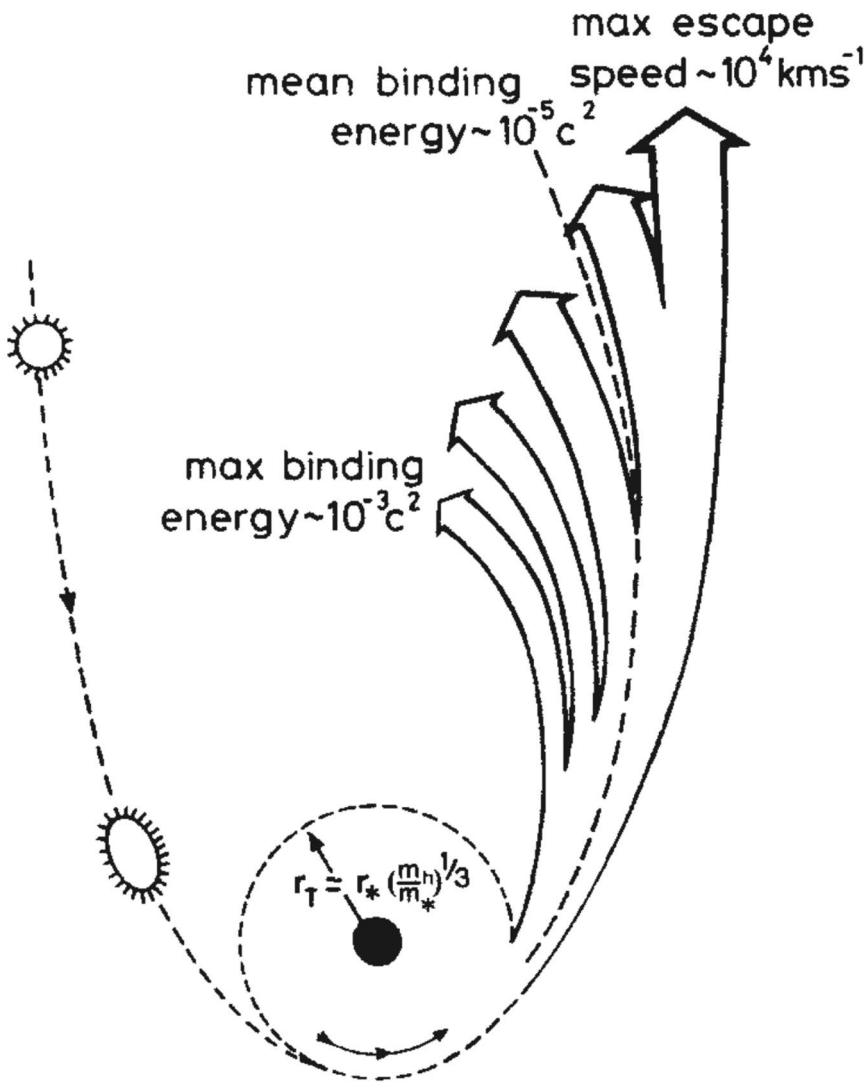

Figure 19. The tidal disruption of a solar-type star by a massive BH. Almost half of the debris created is not bound and instead leaves on a hyperbolic orbit, whilst the rest is circularised and forms an accretion disc (Rees, 1988; Gezari, 2021). Source: Rees (1988).

Though the classical picture involves a SMBH ($> 10^6\,\mathrm{M}_\odot$), TDEs could also

occur under other circumstances, involving intermediate-mass BHs (IMBHs; $10^3 - 10^6\,\mathrm{M}_\odot$) or even stellar-mass BHs ($< 10^3\,\mathrm{M}_\odot$; MacLeod et al. 2016; Mezcua 2017; Kremer et al. 2021; Gutiérrez et al. 2024). The tidal radius, that is, the radius at which a star will become disrupted by tidal forces, is as follows,

$$R_t \approx R_*(\frac{M_h}{M_*})^{\frac{1}{3}} \tag{14}$$

where M_h is the mass of the BH, M_* is the mass of the star and R_* is the radius of the star (Phinney, 1989; Kobayashi et al., 2004). The so-called "penetration factor" is given as follows,

$$\beta = \frac{R_t}{R_p} \tag{15}$$

where R_p is the pericentre distance (Luminet and Pichon, 1989; Rosswog et al., 2009). Tidal disruption will occur for $\beta \gtrsim 1$ (Luminet and Pichon, 1989). As such, given the compactness of WDs, they cannot be disrupted by SMBHs, which is illustrated in Fig. 20 (Luminet and Pichon, 1989; Rosswog et al., 2009).

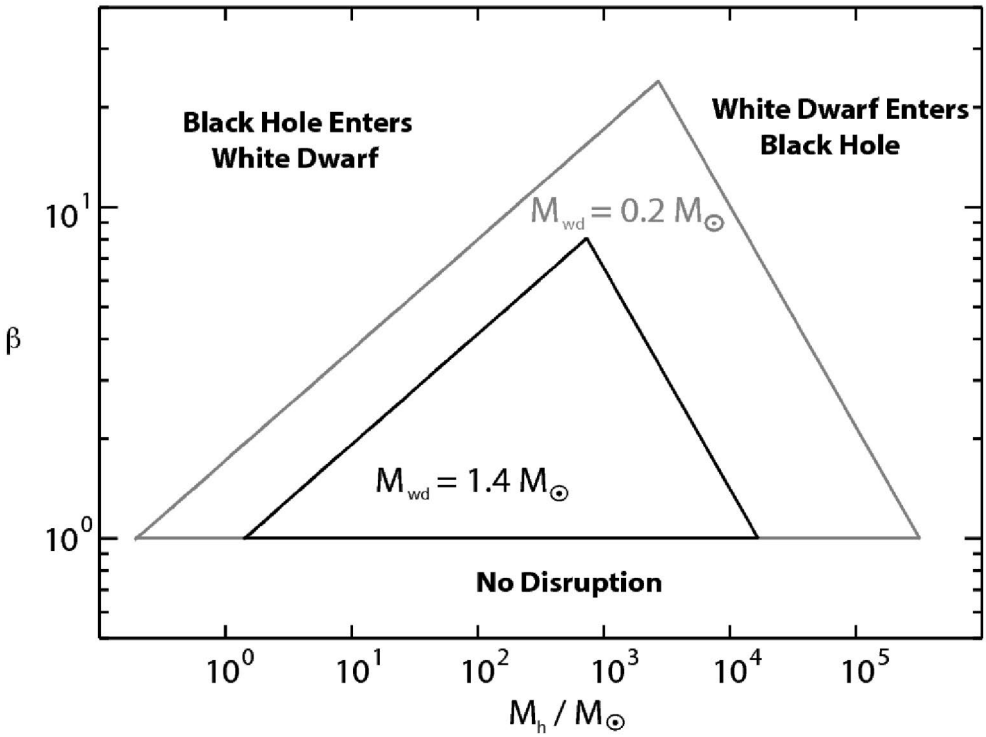

Figure 20. Plot of the penetration factor, β, against BH mass, B_h, in solar masses. The range of values of β and BH masses for which disruption can take place are shown in the case of both a $1.4\,\mathrm{M}_\odot$ WD and a $0.2\,\mathrm{M}_\odot$ WD. It can be seen that SMBHs cannot disrupt WDs. Source: Rosswog et al. (2009).

TDEs are bright in the ultraviolet range, owing to the thermal emission from accretion, and their spectra display blue continua (Arcavi et al., 2014). However, TDEs occupy a continuum of spectral types, ranging from hydrogen-dominated to helium-dominated, with intermediate types showing evidence of both features (Arcavi et al., 2014).

Given that the light curves of TDEs are expected to be accretion powered, we would expect a decline rate of $t^{-5/3}$ (Phinney, 1989). However, it should be noted that this would specifically be expected for the bolometric light curve, and naturally, individual bands may display differing rates (Strubbe and Quataert, 2009). Furthermore, a number of other considerations can impact the decline rate, such as the nature of the density profile (Lodato et al., 2009). Additionally, analytical modelling indicates that the $t^{-5/3}$ decline rate should only hold at late times after the luminosity of the TDE has dropped by two to three magnitudes (Lodato et al., 2009).

TDEs are conceivably a way of finding IMBHs, which are of much interest, given their proposed role in seeding the SMBHs seen at high redshift (Lin et al., 2018; Di Matteo et al., 2023; Gutiérrez et al., 2024). Moreover, TDEs are observationally important as they can serve as a probe of otherwise non-accreting BHs and, indeed, may be the only potential probes of accretion in the case of IMBHs (Gezari, 2021; Angus et al., 2022). Additionally, they provide great insight into accretion physics, given the interaction of the debris streams and the circularisation of the material into an accretion disc along with jet formation (Shen and Matzner, 2014; Gezari, 2021).

5 Summary of the Papers

In this chapter I will provide an overview of the contents of the research papers contained in this thesis. The papers present novel data sets for unique astronomical objects, helping to shed light on various areas of the parameter space of transients in terms of duration, luminosity and physical origin. Interacting SNe, USSNe, TDEs and gap transients such as ILRTs and LRNe are addressed, all having broader implications for stellar evolution.

5.1 Paper I

The first paper concerns the long-lived type IIn SN 2017hcc and provides the results of a five-year follow-up campaign of the object with optical and near-infrared imaging and spectroscopy. SN 2017hcc was a slowly evolving object, both photometrically and spectroscopically. It displayed a long rise time of around eight weeks and reached peak absolute magnitude of -20.78 ± 0.01 in ATLAS o band, indicative of significant interaction between massive ejecta and massive and dense CSM. Not long after maximum light, the object began to display an infrared excess. The object exhibited blueshifted Balmer lines from a few hundred days until around +1200 days post explosion. We plotted the evolution of the centroid of Hα over time in order to demonstrate the evolution in its position.

I was the first author of this paper and wrote the vast majority of the text, reduced most of the data and was principally responsible for the analysis and overall material in the paper. I also responded to the referee.

The extensive data set in this paper allows for a thorough examination of a high-energy explosion in massive and dense CSM. Observations of ejecta-CSM interaction in such events allow for the probing of the production mechanisms and history of the CSM; such observations offer insight into the evolution of massive stars in general, as does distinguishing between the presence of pre-existing dust, indicative of mass loss, and the formation of new dust after the explosion.

5.2 Paper II

The second paper concerns the intermediate-luminosity red transient AT 2022fnm. The observational overlap between LRNe and ILRTs is addressed. In particular, the

evolution of LRN and ILRT light curves and spectra is compared along with rise times and decay rates.

The object did not display the double-peaked feature typical of LRNe, nor did the spectra show the forest of metal lines in absorption or the late-time molecular bands associated with LRNe. The spectra featured the [Ca II] $\lambda\lambda$7291,7323 doublet, which is characteristic of ILRTs, though it was weak. The Ca II λ8498,8542,8662 NIR triplet found in both ILRTs and LRNe was also present. The presence of a near-infrared excess is evident from around +100 d, and we suggest that this results from a dust echo. The spectra also show evidence of ejecta-CSM interaction at late times.

We employed a simple analytical diffusion model to reproduce the pseudo-bolometric light curve of the event and found it to be compatible with ECSNe, though the parameters were degenerate and compatible with a wide variety of scenarios. We concluded that AT 2022fnm is likely the result of a weak stellar explosion or eruption.

I was also the first author of this paper and wrote almost the entirety of the text. Additionally, I am responsible for the majority of the analysis and overall material in the paper and responded to the referee.

This paper serves to comb the parameter space of LRNe and ILRTs, highlighting the similarities between such gap transients, whilst also clarifying the differences in their underlying explosions mechanisms. Improved understanding of objects such as AT 2022fnm helps provide a clearer picture of observationally "transitional" events, though the paper also emphasises the need for higher cadence optical and near-infrared photometry and spectroscopy in order to more clearly discriminate between potential origin pathways.

5.3 Paper III

The third paper concerns the fast-evolving transient SN 2017fwm/Gaia17byh. The object displayed an extremely fast rise time ($\lesssim$5 days) and a small ejecta mass ($0.01\,M_{\odot}$).

The +17 d spectrum of the object was compared against the +23 d spectrum ultrastripped SN 2010X, and a peculiar velocity of $-4{,}980$ km s^{-1} was found after correction for galactic redshift. Various scenarios were investigated in an attempt to explain this object's origins, such as the explosion of a star dynamically ejected by a SMBH via the Hills mechanism (Hills, 1988), shock-cooling emission from the explosion of a low-mass helium star and the merger of a WD and a BH or NS. Ultimately, the strongest suggestions are that this object was an ultrastripped SN or that it was a TDE with the accretion of the material of a tidally disrupted WD leading to the emission. However, neither of these explanations is entirely satisfying.

I was the second author of this paper. I was responsible for the majority of the analysis of the photometric and spectroscopic evolution and made significant contributions to the text and astrophysical analysis.

This paper provides an overview of a number of different categories of events that can produce low ejecta masses and calcium lines, weighing them up against one another by comparing the physical processes leading to their origins as well as their observational characteristics. Furthermore, the puzzling high-velocity discussed presents challenges to our current understanding of the origins of high-energy transients, spotlighting the need for further research in this area.

6 Future Work

6.1 Surveys and Facilities

We are at the dawn of a new age for large sky surveys. In particular, we can expect great observational progress as a whole new generation of instruments and telescopes see first light. Upcoming wide-field surveys, such as the Legacy Survey of Space and Time (LSST), expected to begin in August 2025[1] at the 8.4 m Simonyi Survey Telescope at the Vera C. Rubin Observatory, will find far larger numbers of objects than ever before, producing ∼10 million alerts per night (LSST Dark Energy Science Collaboration, 2012; LSST Dark Energy Science Collaboration et al., 2021; Thomas et al., 2022; Hambleton et al., 2023). The upcoming Time-Domain Extragalactic Survey (TiDES) will use the 4-metre Multi-Object Spectrograph Telescope (4MOST), which is expected to see first light on the VISTA telescope[2] in 2025 and has a 4.2 square degree field of view (de Jong et al., 2012, 2019; Swann et al., 2019; Mainieri et al., 2024). TiDES will serve to complement all-sky photometric surveys, including LSST, by providing spectroscopic follow-up of extragalactic optical transients, including SNe (Swann et al., 2019). Son of X-Shooter (SoXS), which should see first light in early 2025[3], is a medium-resolution wide-band spectrograph to be mounted on the 3.6 m New Technology Telescope at the La Silla Observatory, operated by the European Southern Observatory in Chile, which will allow for spectral classification and follow-up of many more transients (Schipani et al., 2016).

I hope to use the advanced capabilities of these upcoming facilities to enhance our understanding of events such as interacting SNe, ILRTs and TDEs and to find counterparts to gravitational-wave events, discussed in Section 6.3 ahead. Additionally, I am eager to use these instruments and surveys to uncover entirely new kinds of transients, building a clearer picture of the diversity of the transient parameter space with improved detection and prompt (within minutes) follow-up.

[1] https://www.lsst.org/about/project-status

[2] https://www.eso.org/public/teles-instr/paranal-observatory/surveytelescopes/vista/

[3] https://www.eso.org/public/teles-instr/lasilla/ntt/soxs/

6.2 Modelling

This observational progress is only one part of the story, however. In order to make theoretical progress, we need observations that provide much deeper physical insight. Furthermore, we need improved computational models. The accuracy and usefulness of the simulation of astrophysical systems can be improved by furthering our physical understanding of phenomena and by increasing the complexity of the simulations based on already-understood physics. The primary difficulty is the bottleneck posed by computing constraints. It takes a significant amount of time (tens of millions of CPU hours) to model asymmetric events using huge grids (Vartanyan et al., 2019).

The use of three-dimensional magnetohydrodynamic codes for simulation is now widespread, and whilst there are difficulties in handling angular-momentum transport and magnetic-field amplification when modelling stellar evolution, promising improvements are being made in this area (Müller, 2024). Excellent work is being done with regard to modelling of gap transients such as ILRTs and LRNe, but this needs to be extended to models of higher mass. Currently, the modelling is typically done for low-mass stars, more suitable for describing red novae than LRNe (Shara et al., 2010). Additionally, there is a very large parameter space to investigate, including various mass ratios, orbital separations, eccentricities and evolutionary stages of progenitors.

It has consistently been the case that the pace at which observational data has been gathered has far exceeded the corresponding progress of theoretical modelling, a problem that may only be exacerbated with the coming observational revolution (Gezari, 2021). Indeed, as described above, future surveys will find far greater numbers of transients; however, next-generation instruments will allow for improved classification with more photometric and spectroscopic resources and will enable follow-up with higher cadence. As such, our understanding of the stellar evolutionary processes leading to these events will be enhanced, which will allow for the improvement of the physical underpinnings of the models used to simulate them.

6.3 Multi-Messenger Astronomy

Multi-messenger astronomy, the acquisition and analysis of multiple different kinds of signals originating from the same source, will be of profound importance in the coming years. Comparisons are made not only between different parts of the electromagnetic spectrum, from radio waves to gamma rays, but also including neutrinos (with the IceCube Neutrino Observatory and others; IceCube Collaboration et al. 2006) and gravitational waves (with LIGO-Virgo and KAGRA; Abramovici et al. 1992; Barish 1999; Somiya 2012). As some events are expected to produce all three, the ability to collate these different data is of great value.

The neutrinos detected from SN 1987A alongside the electromagnetic detec-

tions made this the first multimessenger transient detection, and to date it is the only transient event for which there has been a confirmed neutrino detection (DarkSide-20k Collaboration et al., 2021). However, a high-energy neutrino detected in 2019 may have originated from the tidal-disruption event AT 2019dsg (Stein et al., 2021). Moreover, neutrinos were detected from the blazar TXS 0506+056 in 2017, offering hope for future successes with improved instrumentation, such as IceCube-Gen2, which is currently in the technical-design stage and will have greatly improved sensitivity compared with current-generation detectors (IceCube Collaboration et al., 2018; Clark et al., 2021; Aartsen et al., 2021). Additionally, future dark-matter detectors, such as the liquid-argon detectors DarkSide-20k and Argo, will also be sensitive to neutrinos, increasing the likelihood of detections and offering enhanced distance determination (to a precision of $\sim 5\%$; DarkSide-20k Collaboration et al. 2021).

The gravitational-wave event GW 170817, corresponding to the merger of a NS binary, was detected on the 17th of August 2017, by the LIGO and Virgo detectors and the multimessenger data provided unprecedented insight into the process (Abbott et al., 2017b). Unfortunately, there were no corresponding neutrino detections, though this may have been a viewing-angle effect (Albert et al., 2017). However, a corresponding short gamma-ray burst, GRB170817A, lasting approximately two seconds was detected 1.7 seconds after the initial gravitational-wave detection (Abbott et al., 2017a). Additionally, an optical counterpart, designated AT 2017gfo, was discovered 11 hours after the gravitational-wave detection (Abbott et al., 2017b).

Electromagnetic counterparts of gravitational-wave events are expected to be particularly faint and quickly evolving, making them especially difficult to find (Agudo et al., 2023). This serves to emphasise the importance of high-cadence wide-field follow-up of sufficient depth. Upcoming surveys, instruments and telescopes are particularly well positioned to tackle these challenges, so the field can be expected to undergo significant growth and progress in the near future.

List of References

Aartsen, M.G. et al (2021). IceCube-Gen2: the window to the extreme Universe. *Journal of Physics G Nuclear Physics*, 48(6):060501.

Abbott, B.P. et al (2017a). Gravitational Waves and Gamma-Rays from a Binary Neutron Star Merger: GW170817 and GRB 170817A. *ApJ*, 848(2):L13.

Abbott, B.P. et al (2017b). Multi-messenger Observations of a Binary Neutron Star Merger. *ApJ*, 848(2):L12.

Abramovici, A. et al (1992). LIGO: The Laser Interferometer Gravitational-Wave Observatory. *Science*, 256(5055):325–333.

Adams, F.C. and Laughlin, G. (1997). A dying universe: the long-term fate and evolution of astrophysical objects. *Reviews of Modern Physics*, 69(2):337–372.

Adams, S.M. et al (2016). Almost gone: SN 2008S and NGC 300 2008OT-1 are fainter than their progenitors. *MNRAS*, 460:1645–1657.

Agudo, I. et al (2023). Panning for gold, but finding helium: Discovery of the ultra-stripped supernova SN 2019wxt from gravitational-wave follow-up observations. *A&A*, 675:A201.

Albert, A. et al (2017). Search for High-energy Neutrinos from Binary Neutron Star Merger GW170817 with ANTARES, IceCube, and the Pierre Auger Observatory. *ApJ*, 850(2):L35.

Angus, C.R. et al (2022). A fast-rising tidal disruption event from a candidate intermediate-mass black hole. *Nature Astronomy*, 6:1452–1463.

Arcavi, I. (2017). Hydrogen-Rich Core-Collapse Supernovae. In Alsabti, A.W. and Murdin, P., editors, *Handbook of Supernovae*, page 239.

Arcavi, I. et al (2014). A Continuum of H- to He-rich Tidal Disruption Candidates With a Preference for E+A Galaxies. *ApJ*, 793(1):38.

Arnett, W.D. (1982). Type I supernovae. I - Analytic solutions for the early part of the light curve. *ApJ*, 253:785–797.

Barish, B.C. (1999). The Detection of Gravitational Waves with LIGO. *arXiv e-prints*, pages gr–qc/9905026.

Bellm, E.C. et al (2019). The Zwicky Transient Facility: System Overview, Performance, and First Results. *PASP*, 131(995):018002.

Bionta, R.M. et al (1987). Observation of a neutrino burst in coincidence with supernova 1987A in the Large Magellanic Cloud. *Phys. Rev. Lett.*, 58(14):1494–1496.

Blagorodnova, N. et al (2021). The luminous red nova AT 2018bwo in NGC 45 and its binary yellow supergiant progenitor. *A&A*, 653:A134.

Blagorodnova, N. et al (2017). Common Envelope Ejection for a Luminous Red Nova in M101. *ApJ*, 834(2):107.

Blinnikov, S. (2017). Interacting Supernovae: Spectra and Light Curves. In Alsabti, A.W. and Murdin, P., editors, *Handbook of Supernovae*, page 843.

Bode, M.F. and Evans, A. (1979). Infrared emission by dust grains near variable primary sources. I. General considerations. *A&A*, 73(1-2):113–120.

Branch, D. and Wheeler, J.C. (2017). *Supernova Explosions*.

Burbidge, E.M. et al (1957). Synthesis of the Elements in Stars. *Reviews of Modern Physics*, 29(4):547–650.

Burrows, A. (2000). Supernova explosions in the Universe. *Nature*, 403(6771):727–733.

Cai, Y. et al (2022a). Gap Transients Interacting with Circumstellar Medium. *Universe*, 8(10):493.
Cai, Y.Z. et al (2021). Intermediate-luminosity red transients: Spectrophotometric properties and connection to electron-capture supernova explosions. *A&A*, 654:A157.
Cai, Y.Z. et al (2018). AT 2017be - a new member of the class of intermediate-luminosity red transients. *MNRAS*, 480(3):3424–3445.
Cai, Y.Z. et al (2019). The transitional gap transient AT 2018hso: new insights into the luminous red nova phenomenon. *A&A*, 632:L6.
Cai, Y.Z. et al (2022b). Forbidden hugs in pandemic times. III. Observations of the luminous red nova AT 2021biy in the nearby galaxy NGC 4631. *A&A*, 667:A4.
Cappellaro, E. et al (2015). Supernova rates from the SUDARE VST-OmegaCAM search. I. Rates per unit volume. *A&A*, 584:A62.
Carroll, B.W. and Ostlie, D.A. (2017). *An introduction to modern astrophysics, Second Edition*.
Chabrier, G. (2003). Galactic Stellar and Substellar Initial Mass Function. *PASP*, 115(809):763–795.
Chandrasekhar, S. (1935). The highly collapsed configurations of a stellar mass (Second paper). *MNRAS*, 95:207–225.
Chevalier, R.A. (1981). Hydrodynamic Models of Supernova Explosions. *Fund. Cosmic Phys.*, 7:1–58.
Chevalier, R.A. and Fransson, C. (1994). Emission from Circumstellar Interaction in Normal Type II Supernovae. *ApJ*, 420:268.
Chevalier, R.A. and Fransson, C. (2017). Thermal and Non-thermal Emission from Circumstellar Interaction. In Alsabti, A.W. and Murdin, P., editors, *Handbook of Supernovae*, page 875.
Chomiuk, L. et al (2011). Pan-STARRS1 Discovery of Two Ultraluminous Supernovae at z $\approx$ 0.9. *ApJ*, 743(2):114.
Chugai, N.N. (1997). Supernovae in dense winds. *Ap&SS*, 252:225–236.
Chugai, N.N. et al (2004). The Type IIn supernova 1994W: evidence for the explosive ejection of a circumstellar envelope. *MNRAS*, 352(4):1213–1231.
Clark, B.A., Clark, B.A. and IceCube-Gen2 Collaboration (2021). The IceCube-Gen2 Neutrino Observatory. *Journal of Instrumentation*, 16(10):C10007.
Colgate, S.A. and McKee, C. (1969). Early Supernova Luminosity. *ApJ*, 157:623.
Couderc, P. (1939). Les auréoles lumineuses des Novæ. *Annales d'Astrophysique*, 2:271.
Crotts, A.P.S. (1988). Discovery of Optical Echoes from Supernova 1987A: New Probes of the Large Magellanic Cloud. *ApJ*, 333:L51.
DarkSide-20k Collaboration et al (2021). Sensitivity of future liquid argon dark matter search experiments to core-collapse supernova neutrinos. *J. Cosmology Astropart. Phys.*, 2021(3):043.
De, K. et al (2021). The Peculiar Ca-rich SN2019ehk: Evidence for a Type IIb Core-collapse Supernova from a Low-mass Stripped Progenitor. *ApJ*, 907(1):L18.
de Jong, R.S. et al (2019). 4MOST: Project overview and information for the First Call for Proposals. *The Messenger*, 175:3–11.
de Jong, R.S. et al (2012). 4MOST: 4-metre multi-object spectroscopic telescope. In McLean, I.S., Ramsay, S.K. and Takami, H., editors, *Ground-based and Airborne Instrumentation for Astronomy IV*, volume 8446 of *Society of Photo-Optical Instrumentation Engineers (SPIE) Conference Series*, page 84460T.
Dessart, L. et al (2022). Using LSST late-time photometry to constrain Type Ibc supernovae and their progenitors. *A&A*, 666:L14.
Di Matteo, T. et al (2023). A vast population of wandering and merging IMBHs at cosmic noon. *MNRAS*, 525(1):1479–1497.
Dimitriadis, G., Siebert, M.R. and Foley, R.J. (2020). UCSC Transient Classification Report for 2020-07-24. *Transient Name Server Classification Report*, 2020-2259:1.
Donley, J.L. et al (2002). Large-Amplitude X-Ray Outbursts from Galactic Nuclei: A Systematic Survey using ROSAT Archival Data. *AJ*, 124(3):1308–1321.
Dopita, M.A. and Tuohy, I.R. (1984). Spectrophotometry of young supernova remnants. *ApJ*, 282:135–141.
Eddington, A.S. (1926). *The Internal Constitution of the Stars*.

Eldridge, J.J. et al (2013). The death of massive stars - II. Observational constraints on the progenitors of Type Ibc supernovae. *MNRAS*, 436(1):774–795.

Elias-Rosa, N. et al (2024). SN 2020pvb: A Type IIn-P supernova with a precursor outburst. *A&A*, 686:A13.

Fang, K. et al (2019). Multimessenger Implications of AT2018cow: High-energy Cosmic-Ray and Neutrino Emissions from Magnetar-powered Superluminous Transients. *ApJ*, 878(1):34.

Fassia, A. et al (2000). Optical and infrared photometry of the Type IIn SN 1998S: days 11-146. *MNRAS*, 318(4):1093–1104.

Filippenko, A.V. (1997). Optical Spectra of Supernovae. *ARA&A*, 35:309–355.

Fox, D.W. et al (2003). Discovery of Early Optical Emission from GRB 021211. *ApJ*, 586(1):L5–L8.

Fox, O.D. et al (2011). A Spitzer Survey for Dust in Type IIn Supernovae. *ApJ*, 741(1):7.

Fraser, M. (2020). Supernovae and transients with circumstellar interaction. *Royal Society Open Science*, 7(7):200467.

Fraser, M. et al (2013). SN 2009ip à la PESSTO: no evidence for core collapse yet. *MNRAS*, 433(2):1312–1337.

Gal-Yam, A. (2017). Observational and Physical Classification of Supernovae. In Alsabti, A.W. and Murdin, P., editors, *Handbook of Supernovae*, page 195.

Gehrz, R.D. and Ney, E.P. (1990). Confirmation of Dust Condensation in the Ejecta of Supernova 1987a. *Proceedings of the National Academy of Science*, 87(11):4354–4357.

Gerardy, C.L. et al (2002). Extraordinary Late-Time Infrared Emission of Type IIn Supernovae. *ApJ*, 575(2):1007–1017.

Gezari, S. (2021). Tidal Disruption Events. *ARA&A*, 59:21–58.

Gompertz, B.P. et al (2020). Searching for electromagnetic counterparts to gravitational-wave merger events with the prototype Gravitational-Wave Optical Transient Observer (GOTO-4). *MNRAS*, 497(1):726–738.

Graham, J.R. et al (1983). Discovery of an IR echo from a supernova dust cloud. *Nature*, 304(5928):709–710.

Groenewegen, M.A.T. and Sloan, G.C. (2018). Luminosities and mass-loss rates of Local Group AGB stars and red supergiants. *A&A*, 609:A114.

Gutiérrez, C.P. et al (2024). CSS161010: a luminous, fast blue optical transient with broad blueshifted hydrogen lines. *arXiv e-prints*, page arXiv:2408.04698.

Hambleton, K.M. et al (2023). Rubin Observatory LSST Transients and Variable Stars Roadmap. *PASP*, 135(1052):105002.

Hansen, C.J., Kawaler, S.D. and Trimble, V. (2004). *Stellar interiors : physical principles, structure, and evolution*.

Heger, A. et al (2003). How Massive Single Stars End Their Life. *ApJ*, 591(1):288–300.

Hills, J.G. (1975). Possible power source of Seyfert galaxies and QSOs. *Nature*, 254(5498):295–298.

Hills, J.G. (1988). Hyper-velocity and tidal stars from binaries disrupted by a massive Galactic black hole. *Nature*, 331(6158):687–689.

Hirata, K. et al (1987). Observation of a neutrino burst from the supernova SN1987A. *Phys. Rev. Lett.*, 58(14):1490–1493.

Hoyle, F. and Wickramasinghe, N.C. (1962). On graphite particles as interstellar grains. *MNRAS*, 124:417.

Humphreys, R.M. and Davidson, K. (1984). The Most Luminous Stars. *Science*, 223(4633):243–249.

Humphreys, R.M. and Davidson, K. (1994). The Luminous Blue Variables: Astrophysical Geysers. *PASP*, 106:1025.

Humphreys, R.M. et al (2020). Exploring the Mass-loss Histories of the Red Supergiants. *AJ*, 160(3):145.

IceCube Collaboration et al (2018). Multimessenger observations of a flaring blazar coincident with high-energy neutrino IceCube-170922A. *Science*, 361(6398):eaat1378.

IceCube Collaboration et al (2006). First year performance of the IceCube neutrino telescope. *Astroparticle Physics*, 26(3):155–173.

Inserra, C. (2019). Observational properties of extreme supernovae. *Nature Astronomy*, 3:697–705.

Israelian, G. and de Groot, M. (1999). P Cygni: An Extraordinary Luminous Blue Variable. *Space Sci. Rev.*, 90:493–522.

Ivanova, N. et al (2013). Common envelope evolution: where we stand and how we can move forward. *A&A Rev.*, 21:59.

Jacobson-Galán, W.V. et al (2020). SN 2019ehk: A Double-peaked Ca-rich Transient with Luminous X-Ray Emission and Shock-ionized Spectral Features. *ApJ*, 898(2):166.

Janka, H.T. et al (2012). Core-collapse supernovae: Reflections and directions. *Progress of Theoretical and Experimental Physics*, 2012(1):01A309.

Janka, H.T. et al (2007). Theory of core-collapse supernovae. *Phys. Rep.*, 442(1-6):38–74.

Jerkstrand, A. (2017). Spectra of Supernovae in the Nebular Phase. In Alsabti, A.W. and Murdin, P., editors, *Handbook of Supernovae*, page 795.

Kankare, E. et al (2012). SN 2009kn - the twin of the Type IIn supernova 1994W. *MNRAS*, 424(2):855–873.

Karakas, A.I. (2017). Low- and Intermediate-Mass Stars. In Alsabti, A.W. and Murdin, P., editors, *Handbook of Supernovae*, page 461.

Kasen, D. (2017). Unusual Supernovae and Alternative Power Sources. In Alsabti, A.W. and Murdin, P., editors, *Handbook of Supernovae*, page 939.

Kashi, A., Frankowski, A. and Soker, N. (2010). NGC 300 OT2008-1 as a Scaled-down Version of the Eta Carinae Great Eruption. *ApJ*, 709(1):L11–L15.

Kasliwal, M.M. et al (2012). Calcium-rich Gap Transients in the Remote Outskirts of Galaxies. *ApJ*, 755(2):161.

Kaspi, V.M. and Beloborodov, A.M. (2017). Magnetars. *ARA&A*, 55(1):261–301.

Kiewe, M. et al (2012). Caltech Core-Collapse Project (CCCP) Observations of Type IIn Supernovae: Typical Properties and Implications for Their Progenitor Stars. *ApJ*, 744(1):10.

Kippenhahn, R., Weigert, A. and Weiss, A. (2013). *Stellar Structure and Evolution*.

Kirshner, R.P. and Kwan, J. (1974). Distances to extragalactic supernovae. *ApJ*, 193:27–36.

Kirshner, R.P. et al (1973). The spectra of supernovae. *ApJ*, 185:303.

Kobayashi, S. et al (2004). Gravitational Waves and X-Ray Signals from Stellar Disruption by a Massive Black Hole. *ApJ*, 615(2):855–865.

Kochanek, C.S., Adams, S.M. and Belczynski, K. (2014). Stellar mergers are common. *MNRAS*, 443(2):1319–1328.

Kochanek, C.S. et al (2017). The All-Sky Automated Survey for Supernovae (ASAS-SN) Light Curve Server v1.0. *PASP*, 129(980):104502.

Komossa, S. (2015). Tidal disruption of stars by supermassive black holes: Status of observations. *Journal of High Energy Astrophysics*, 7:148–157.

Kotak, R. et al (2004). On the nature of the circumstellar medium of the remarkable Type Ia/IIn supernova SN 2002ic. *MNRAS*, 354(2):L13–L17.

Kotak, R. et al (2009). Dust and The Type II-Plateau Supernova 2004et. *ApJ*, 704(1):306–323.

Kotak, R. and Vink, J.S. (2006). Luminous blue variables as the progenitors of supernovae with quasi-periodic radio modulations. *A&A*, 460(2):L5–L8.

Kratz, K.L., Farouqi, K. and Möller, P. (2014). A High-entropy-wind r-process Study Based on Nuclear-structure Quantities from the New Finite-range Droplet Model Frdm(2012). *ApJ*, 792(1):6.

Kremer, K. et al (2021). Fast Optical Transients from Stellar-mass Black Hole Tidal Disruption Events in Young Star Clusters. *ApJ*, 911(2):104.

Kuiper, G.P. (1938). The Empirical Mass-Luminosity Relation. *ApJ*, 88:472.

Lamers, H.J.G.L.M. and Cassinelli, J.P. (1999). *Introduction to Stellar Winds*.

Langer, N. (2012). Presupernova Evolution of Massive Single and Binary Stars. *ARA&A*, 50:107–164.

Langer, N., Wellstein, S. and Petrovic, J. (2003). On the evolution of massive close binaries. In van der Hucht, K., Herrero, A. and Esteban, C., editors, *A Massive Star Odyssey: From Main Sequence to Supernova*, volume 212, page 275.

Leonard, D.C. et al (2000). Evidence for Asphericity in the Type IIN Supernova SN 1998S. *ApJ*, 536(1):239–254.

Levesque, E.M. et al (2014). The Peculiar Balmer Decrement of SN 2009ip: Constraints on Circumstellar Geometry. *AJ*, 147(1):23.

Li, C. and Morozova, V. (2022). Modelling the light curve of Type IIn-P SN 2005cl with red supergiant progenitors featuring pre-SN outbursts. *MNRAS*, 515(3):3597–3602.

Li, W. et al (2011). Nearby supernova rates from the Lick Observatory Supernova Search - II. The observed luminosity functions and fractions of supernovae in a complete sample. *MNRAS*, 412:1441–1472.

Lin, D. et al (2018). A luminous X-ray outburst from an intermediate-mass black hole in an off-centre star cluster. *Nature Astronomy*, 2:656–661.

Lodato, G., King, A.R. and Pringle, J.E. (2009). Stellar disruption by a supermassive black hole: is the light curve really proportional to $t^{-5/3}$? *MNRAS*, 392(1):332–340.

Lodders, K. and Fegley, B., J. (1995). The origin of circumstellar silicon carbide grains found in meteorites. *Meteoritics*, 30(6):661.

LSST Dark Energy Science Collaboration (2012). Large Synoptic Survey Telescope: Dark Energy Science Collaboration. *arXiv e-prints*, page arXiv:1211.0310.

LSST Dark Energy Science Collaboration et al (2021). The LSST DESC DC2 Simulated Sky Survey. *ApJS*, 253(1):31.

Lucy, L.B. et al (1989). Dust Condensation in the Ejecta of SN 1987 A. In Tenorio-Tagle, G., Moles, M. and Melnick, J., editors, *IAU Colloq. 120: Structure and Dynamics of the Interstellar Medium*, volume 350, page 164.

Lucy, L.B. and Solomon, P.M. (1970). Mass Loss by Hot Stars. *ApJ*, 159:879.

Luminet, J.P. and Pichon, B. (1989). Tidal pinching of white dwarfs. *A&A*, 209(1-2):103–110.

Lunnan, R. et al (2017). Two New Calcium-rich Gap Transients in Group and Cluster Environments. *ApJ*, 836(1):60.

Lyman, J.D. et al (2016). Hubble Space Telescope observations of the host galaxies and environments of calcium-rich supernovae. *MNRAS*, 458(2):1768–1777.

MacLeod, M. et al (2016). Optical Thermonuclear Transients from Tidal Compression of White Dwarfs as Tracers of the Low End of the Massive Black Hole Mass Function. *ApJ*, 819(1):3.

MacLeod, M. et al (2017). Lessons from the Onset of a Common Envelope Episode: the Remarkable M31 2015 Luminous Red Nova Outburst. *ApJ*, 835(2):282.

Maeder, A. and Meynet, G. (2000). The Evolution of Rotating Stars. *ARA&A*, 38:143–190.

Mainieri, V. et al (2024). The Wide-field Spectroscopic Telescope (WST) Science White Paper. *arXiv e-prints*, page arXiv:2403.05398.

Mason, E. et al (2010). The peculiar nova V1309 Scorpii/nova Scorpii 2008. A candidate twin of V838 Monocerotis. *A&A*, 516:A108.

Matsumoto, T. and Metzger, B.D. (2022). Light-curve Model for Luminous Red Novae and Inferences about the Ejecta of Stellar Mergers. *ApJ*, 938(1):5.

Matsuura, M. (2017). Dust and Molecular Formation in Supernovae. In Alsabti, A.W. and Murdin, P., editors, *Handbook of Supernovae*, page 2125.

Mattila, S. et al (2012). Core-collapse Supernovae Missed by Optical Surveys. *ApJ*, 756(2):111.

Mattila, S. et al (2008). Massive stars exploding in a He-rich circumstellar medium - III. SN 2006jc: infrared echoes from new and old dust in the progenitor CSM. *MNRAS*, 389(1):141–155.

Mattila, S. et al (2018). A dust-enshrouded tidal disruption event with a resolved radio jet in a galaxy merger. *Science*, 361(6401):482–485.

Mauerhan, J.C. et al (2013). SN 2011ht: confirming a class of interacting supernovae with plateau light curves (Type IIn-P). *MNRAS*, 431(3):2599–2611.

Mereghetti, S., Pons, J.A. and Melatos, A. (2015). Magnetars: Properties, Origin and Evolution. *Space Sci. Rev.*, 191(1-4):315–338.

Metzger, B.D. et al (2010). Electromagnetic counterparts of compact object mergers powered by the radioactive decay of r-process nuclei. *MNRAS*, 406(4):2650–2662.

Metzger, B.D. and Pejcha, O. (2017). Shock-powered light curves of luminous red novae as signatures of pre-dynamical mass-loss in stellar mergers. *MNRAS*, 471(3):3200–3211.

Mezcua, M. (2017). Observational evidence for intermediate-mass black holes. *International Journal of Modern Physics D*, 26(11):1730021.

Miller, A.A. et al (2010). SN 2008iy: an unusual Type IIn Supernova with an enduring 400-d rise time. *MNRAS*, 404(1):305–317.

Minkowski, R. (1941). Spectra of Supernovae. *PASP*, 53(314):224.

Moriya, T.J. et al (2017). Light-curve and spectral properties of ultrastripped core-collapse supernovae leading to binary neutron stars. *MNRAS*, 466(2):2085–2098.

Müller, B. (2024). Supernova Simulations. *arXiv e-prints*, page arXiv:2403.18952.

Myra, E.S. and Burrows, A. (1990). Neutrinos from Type II Supernovae: The First 100 Milliseconds. *ApJ*, 364:222.

Nakaoka, T. et al (2021). Calcium-rich Transient SN 2019ehk in a Star-forming Environment: Yet Another Candidate for a Precursor of a Double Neutron-star Binary. *ApJ*, 912(1):30.

Nomoto, K. (1984). Evolution of 8-10 solar mass stars toward electron capture supernovae. I - Formation of electron-degenerate O + NE + MG cores. *ApJ*, 277:791–805.

Nomoto, K. and Leung, S.C. (2017). Electron Capture Supernovae from Super Asymptotic Giant Branch Stars. In Alsabti, A.W. and Murdin, P., editors, *Handbook of Supernovae*, page 483.

Nugis, T. and Lamers, H.J.G.L.M. (2000). Mass-loss rates of Wolf-Rayet stars as a function of stellar parameters. *A&A*, 360:227–244.

Ofek, E.O. et al (2019). A Six-year Image-subtraction Light Curve of SN2010jl. *PASP*, 131(999):054204.

Osterbrock, D.E. (1989). *Astrophysics of gaseous nebulae and active galactic nuclei*.

Owocki, S. and van Marle, A.J. (2008). Luminous Blue Variables & Mass Loss near the Eddington Limit. In Bresolin, F., Crowther, P.A. and Puls, J., editors, *Massive Stars as Cosmic Engines*, volume 250 of *IAU Symposium*, pages 71–82.

Owocki, S.P., Gayley, K.G. and Shaviv, N.J. (2004). A Porosity-Length Formalism for Photon-Tiring-limited Mass Loss from Stars above the Eddington Limit. *ApJ*, 616(1):525–541.

Paczyński, B. (1971). Evolutionary Processes in Close Binary Systems. *ARA&A*, 9:183.

Paczynski, B. (1976). Common Envelope Binaries. In Eggleton, P., Mitton, S. and Whelan, J., editors, *Structure and Evolution of Close Binary Systems*, volume 73 of *IAU Symposium*, page 75.

Pastorello, A. and Fraser, M. (2019). Supernova impostors and other gap transients. *Nature Astronomy*, 3:676–679.

Pastorello, A. et al (2019). Luminous red novae: Stellar mergers or giant eruptions? *A&A*, 630:A75.

Pastorello, A. et al (2023). Forbidden hugs in pandemic times. IV. Panchromatic evolution of three luminous red novae. *A&A*, 671:A158.

Perets, H.B. et al (2010). A faint type of supernova from a white dwarf with a helium-rich companion. *Nature*, 465(7296):322–325.

Phinney, E.S. (1989). Manifestations of a Massive Black Hole in the Galactic Center. In Morris, M., editor, *The Center of the Galaxy*, volume 136, page 543.

Podsiadlowski, P. (2017). The Progenitor of SN 1987A. In Alsabti, A.W. and Murdin, P., editors, *Handbook of Supernovae*, page 635.

Podsiadlowski, P. et al (2004). The Effects of Binary Evolution on the Dynamics of Core Collapse and Neutron Star Kicks. *ApJ*, 612(2):1044–1051.

Poelarends, A.J.T. et al (2008). The Supernova Channel of Super-AGB Stars. *ApJ*, 675(1):614–625.

Pumo, M.L. et al (2009). EC-SNe from Super-Asymptotic Giant Branch Progenitors: Theoretical Models Versus Observations. *ApJ*, 705(2):L138–L142.

Ransome, C.L. et al (2021). A systematic reclassification of Type IIn supernovae. *MNRAS*, 506(4):4715–4734.

Rees, M.J. (1988). Tidal disruption of stars by black holes of 10^6-10^8 solar masses in nearby galaxies. *Nature*, 333(6173):523–528.

Reguitti, A. et al (2024). Searching for precursor activity of Type IIn Supernovae. *arXiv e-prints*, page arXiv:2403.10398.

Reimers, D. (1975). Circumstellar absorption lines and mass loss from red giants. *Memoires of the Societe Royale des Sciences de Liege*, 8:369–382.

Rodriguez, O., Nakar, E. and Maoz, D. (2024). Stripped-envelope supernova light curves argue for central engine activity. *Nature*, 628:733–735.

Rosswog, S., Ramirez-Ruiz, E. and Hix, W.R. (2009). Tidal Disruption and Ignition of White Dwarfs by Moderately Massive Black Holes. *ApJ*, 695(1):404–419.

Salpeter, E.E. (1955). The Luminosity Function and Stellar Evolution. *ApJ*, 121:161.

Scheck, L. et al (2006). Multidimensional supernova simulations with approximative neutrino transport. I. Neutron star kicks and the anisotropy of neutrino-driven explosions in two spatial dimensions. *A&A*, 457(3):963–986.

Schipani, P. et al (2016). The new SOXS instrument for the ESO NTT. In Evans, C.J., Simard, L. and Takami, H., editors, *Ground-based and Airborne Instrumentation for Astronomy VI*, volume 9908 of *Society of Photo-Optical Instrumentation Engineers (SPIE) Conference Series*, page 990841.

Schlegel, E.M. (1990). A new subclass of type II supernovae? *MNRAS*, 244:269–271.

Shappee, B.J. et al (2014). The Man behind the Curtain: X-Rays Drive the UV through NIR Variability in the 2013 Active Galactic Nucleus Outburst in NGC 2617. *ApJ*, 788(1):48.

Shara, M.M. et al (2010). An Extended Grid of Nova Models. III. Very Luminous, Red Novae. *ApJ*, 725(1):831–841.

Shen, R.F. and Matzner, C.D. (2014). Evolution of Accretion Disks in Tidal Disruption Events. *ApJ*, 784(2):87.

Sieverding, A. et al (2021). Impact of Dark Photon Emission on Massive Star Evolution and Pre-supernova Neutrino Signal. *ApJ*, 912(1):13.

Smith, K.W. et al (2020). Design and Operation of the ATLAS Transient Science Server. *PASP*, 132(1014):085002.

Smith, N. (2013). The Crab nebula and the class of Type IIn-P supernovae caused by sub-energetic electron-capture explosions. *MNRAS*, 434(1):102–113.

Smith, N. (2014). Mass Loss: Its Effect on the Evolution and Fate of High-Mass Stars. *ARA&A*, 52:487–528.

Smith, N. (2017). Interacting Supernovae: Types IIn and Ibn. In Alsabti, A.W. and Murdin, P., editors, *Handbook of Supernovae*, page 403.

Smith, N. et al (2009). SN 2008S: A Cool Super-Eddington Wind in a Supernova Impostor. *ApJ*, 697(1):L49–L53.

Smith, N. and Owocki, S.P. (2006). On the Role of Continuum-driven Eruptions in the Evolution of Very Massive Stars and Population III Stars. *ApJ*, 645(1):L45–L48.

Somiya, K. (2012). Detector configuration of KAGRA-the Japanese cryogenic gravitational-wave detector. *Classical and Quantum Gravity*, 29(12):124007.

Stanek, K.Z. and Kochanek, C.S. (2020). ASAS-SN Transient Discovery Report for 2020-06-30. *Transient Name Server Discovery Report*, 2020-1987:1.

Stanway, E.R., Eldridge, J.J. and Chrimes, A.A. (2020). Binary fraction indicators in resolved stellar populations and supernova-type ratios. *MNRAS*, 497(2):2201–2212.

Steeghs, D. et al (2022). The Gravitational-wave Optical Transient Observer (GOTO): prototype performance and prospects for transient science. *MNRAS*, 511(2):2405–2422.

Stein, R. et al (2021). A tidal disruption event coincident with a high-energy neutrino. *Nature Astronomy*, 5:510–518.

Stritzinger, M.D. et al (2020). The Carnegie Supernova Project II. Observations of the intermediate-luminosity red transient SNhunt120. *A&A*, 639:A103.

Strubbe, L.E. and Quataert, E. (2009). Optical flares from the tidal disruption of stars by massive black holes. *MNRAS*, 400(4):2070–2084.

Swann, E. et al (2019). 4MOST Consortium Survey 10: The Time-Domain Extragalactic Survey (TiDES). *The Messenger*, 175:58–61.

Tanvir, N.R. et al (2009). A γ-ray burst at a redshift of z$\sim$8.2. *Nature*, 461(7268):1254–1257.

Taubenberger, S. et al (2009). Nebular emission-line profiles of Type Ib/c supernovae - probing the ejecta asphericity. *MNRAS*, 397(2):677–694.

Tauris, T.M. et al (2017). Formation of Double Neutron Star Systems. *ApJ*, 846(2):170.

Tauris, T.M. et al (2013). Ultra-stripped Type Ic Supernovae from Close Binary Evolution. *ApJ*, 778(2):L23.

Tauris, T.M., Langer, N. and Podsiadlowski, P. (2015). Ultra-stripped supernovae: progenitors and fate. *MNRAS*, 451(2):2123–2144.

Thielemann, F.K. et al (2011). What are the astrophysical sites for the r-process and the production of heavy elements? *Progress in Particle and Nuclear Physics*, 66(2):346–353.

Thielemann, F.K. et al (2017). Making the Heaviest Elements in a Rare Class of Supernovae. In Alsabti, A.W. and Murdin, P., editors, *Handbook of Supernovae*, page 1843.

Thomas, S.J. et al (2022). Rubin Observatory Simonyi Survey Telescope status overview. In Marshall, H.K., Spyromilio, J. and Usuda, T., editors, *Ground-based and Airborne Telescopes IX*, volume 12182 of *Society of Photo-Optical Instrumentation Engineers (SPIE) Conference Series*, page 121820W.

Thompson, T.A. et al (2009). A New Class of Luminous Transients and a First Census of their Massive Stellar Progenitors. *ApJ*, 705(2):1364–1384.

Tielens, A.G.G.M., Waters, L.B.F.M. and Bernatowicz, T.J. (2005). Origin and Evolution of Dust in Circumstellar and Interstellar Environments. In Krot, A.N., Scott, E.R.D. and Reipurth, B., editors, *Chondrites and the Protoplanetary Disk*, volume 341 of *Astronomical Society of the Pacific Conference Series*, page 605.

Tonry, J.L. et al (2018). ATLAS: A High-cadence All-sky Survey System. *PASP*, 130(988):064505.

Tylenda, R. et al (2011). V1309 Scorpii: merger of a contact binary. *A&A*, 528:A114.

Vartanyan, D. et al (2019). A successful 3D core-collapse supernova explosion model. *MNRAS*, 482(1):351–369.

Waxman, E. and Katz, B. (2017). Shock Breakout Theory. In Alsabti, A.W. and Murdin, P., editors, *Handbook of Supernovae*, page 967.

Wheeler, J.C., Cowan, J.J. and Hillebrandt, W. (1998). The r-Process in Collapsing O/Ne/Mg Cores. *ApJ*, 493(2):L101–L104.

Wooden, D.H. et al (1993). Airborne Spectrophotometry of SN 1987A from 1.7 to 12.6 Microns: Time History of the Dust Continuum and Line Emission. *ApJS*, 88:477.

Woosley, S. and Janka, T. (2005). The physics of core-collapse supernovae. *Nature Physics*, 1(3):147–154.

Yao, Y. et al (2020). SN2019dge: A Helium-rich Ultra-stripped Envelope Supernova. *ApJ*, 900(1):46.

TURUN
YLIOPISTO
UNIVERSITY
OF TURKU

Painosalama, Turku, Finland 2025

ISBN 978-952-02-0052-7 (PRINT)
ISBN 978-952-02-0053-4 (PDF)
ISSN 0082-7002 (PRINT)
ISSN 2343-3175 (ONLINE)